Article

Cell Reports

# Cell Lineage Tracing Identifies Hormone-Regulated and Wnt-Responsive Vaginal Epithelial Stem Cells

## Graphical Abstract

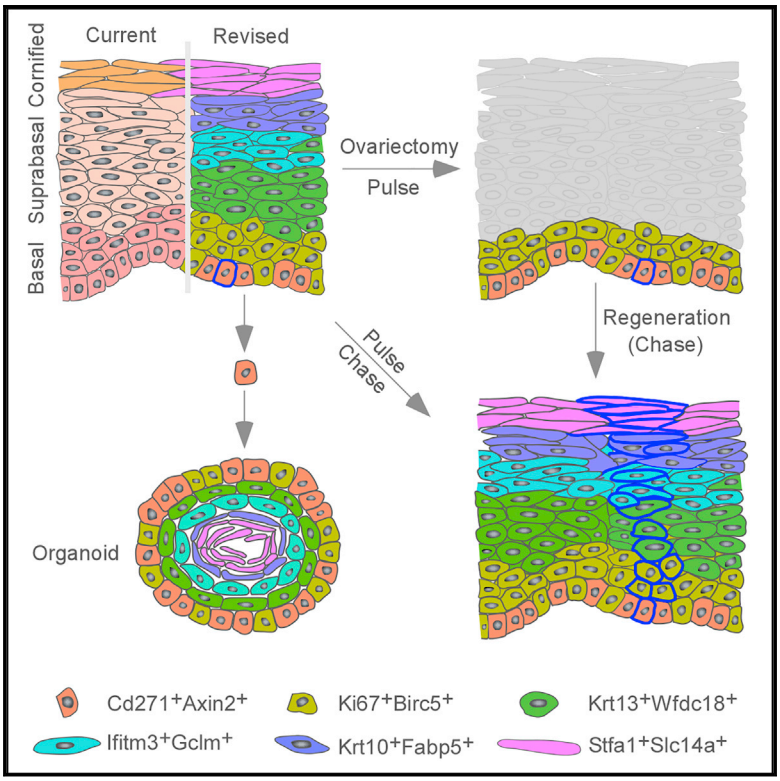


## Highlights

- scRNA-seq analysis redefines vaginal epithelial cell hierarchy
- Cd271+Axin2+ cells represent ovariectomy-resistant vaginal epithelial stem cells
- These cells are responsible for vaginal epithelial homeostasis and regeneration
- Cd271+Axin2+ cell-derived organoids mimic vaginal epithelium in vivo

## Authors

Ayesha Ali, Shafiq M. Syed, M. Fairuz B. Jamaluddin, Yolanda Colino-Sanguino, David Gallego-Ortega, Pradeep S. Tanwar

## Correspondence

pradeep.tanwar@newcastle.edu.au

## In Brief

Abnormalities in vaginal epithelium, the first line of defense against pathogens, are associated with sexually transmitted diseases and vaginal atrophy. Ali et al. show that CD271+Axin2+ basal cells are vaginal stem cells that are responsible for epithelial homeostasis and regeneration, providing fundamental insights into the maintenance of this epithelial barrier.

Ali et al., 2020, Cell Reports *30*, 1463–1477
February 4, 2020 
https://doi.org/10.1016/j.celrep.2020.01.003

CellPress

Cell Reports
Article



# Cell Lineage Tracing Identifies Hormone-Regulated and Wnt-Responsive Vaginal Epithelial Stem Cells

Ayesha Ali,[1,2] Shafiq M. Syed,[1,2] M. Fairuz B. Jamaluddin,[1,2] Yolanda Colino-Sanguino,[3] David Gallego-Ortega,[4,5] and Pradeep S. Tanwar[1,2,6,*]

[1]School of Biomedical Sciences and Pharmacy, University of Newcastle, Callaghan, 2308 NSW, Australia
[2]Hunter Medical Research Institute, New Lambton Heights, 2305 NSW, Australia
[3]Genomic and Epigenetics Group, The Kinghorn Cancer Centre, Garvan Institute of Medical Research, Darlinghurst, 2010 NSW, Australia
[4]Tumour Development Group, The Kinghorn Cancer Centre, Garvan Institute of Medical Research, Darlinghurst, 2010 NSW, Australia
[5]St. Vincent's Clinical School, University of New South Wales, Sydney, 2010 NSW, Australia
[6]Lead Contact
*Correspondence: pradeep.tanwar@newcastle.edu.au
https://doi.org/10.1016/j.celrep.2020.01.003

## SUMMARY

**The intact vaginal epithelium is essential for women's reproductive health and provides protection against HIV and sexually transmitted infections. How this epithelium maintains itself remains poorly understood. Here, we used single-cell RNA sequencing (RNA-seq) to define the diverse cell populations in the vaginal epithelium. We show that vaginal epithelial cell proliferation is limited to the basal compartment without any obvious label-retaining cells. Furthermore, we developed vaginal organoids and show that the basal cells have increased organoid forming efficiency. Importantly, Axin2 marks a self-renewing subpopulation of basal cells that gives rise to differentiated cells over time. These cells are ovariectomy-resistant stem cells as they proliferate even in the absence of hormones. Upon hormone supplementation, these cells expand and reconstitute the entire vaginal epithelium. Wnt/β-catenin is essential for the proliferation and differentiation of vaginal stem cells. Together, these data define heterogeneity in vaginal epithelium and identify vaginal epithelial stem cells.**

## INTRODUCTION

Vaginal epithelium (VE) is a keratinized stratified squamous epithelium consisting of three layers: basal layer, suprabasal layer, and apical cornified layer (Bragulla and Homberger, 2009). The VE lining is highly sensitive to modulation in estrogen (E2) levels (Gardner, 1959) and plays a vital role in various reproductive processes, presenting the first line of defense against the pathogenic invasion in lower reproductive tract (Lee et al., 2016). Experimental or age-related decline in E2 levels in mice and humans leads to regression of VE, which is reversed upon the external supplementation of E2 (Edgren, 1959). This exceptional regenerative capacity of VE suggests the existence of a population of epithelial stem/progenitor cells. However, the identity and location of such cells is currently unknown.

Wnt signaling is an important regulator of various stages of female reproductive tract development and is a known master controller of adult stem cell maintenance in many organ systems (Kobayashi and Behringer, 2003; Nusse, 2008). Various studies in human patients and mouse models have established that deregulated Wnt signaling causes developmental defects and diseases of reproductive tract organs (Ghosh et al., 2017; Goad et al., 2017; Tanwar et al., 2010). Currently, very little is known about the role of Wnt signaling in VE homeostasis.

In this study, using genetic cell lineage tracing, vaginal organoid culture, targeted gene deletion, and single-cell sequencing approaches, we revealed a unique population of VE stem cells and provided evidence that canonical Wnt/β-catenin signaling is required for the proliferation and differentiation of these stem cells.

## RESULTS

### Analysis of Vaginal Epithelial Cells Using Single-Cell Sequencing

To understand the overall diversity of cell types in VE, we performed unbiased single-cell RNA sequencing (scRNA-seq) analysis on mouse VE cells from 5 mice in duplicate. A total of 4,940 cells, of the combined duplicates, that passed QC filtering were clustered into six cell clusters using the k-means method and visualized using t-Distributed Stochastic Neighbor Embedding (tSNE) projection (clusters 0–5; Figures 1A and 1B; Table S1). Differential gene expression and canonical pathway analysis revealed that cluster 0 is enriched for the signaling pathways (Wnt, Integrin, and Death receptor signaling) that are involved in the regulation of various other epithelial stem/progenitor cells and also expresses some of the known stem/progenitor cell markers (Col17a1: collagen type XVII alpha 1 and Igfbp2: insulin-like growth factor binding protein 2) of other organ systems (Plasschaert et al., 2018; Tanimura et al., 2011) (Figures 1A–1C). Cluster 1 represented a population of proliferating cells (Ki67, Top2a, and Birc5) and showed upregulation of signaling pathways involved in mitosis and DNA replication (Figures 1B–1D). Clusters 2 and 3 represented cells in the state of transition

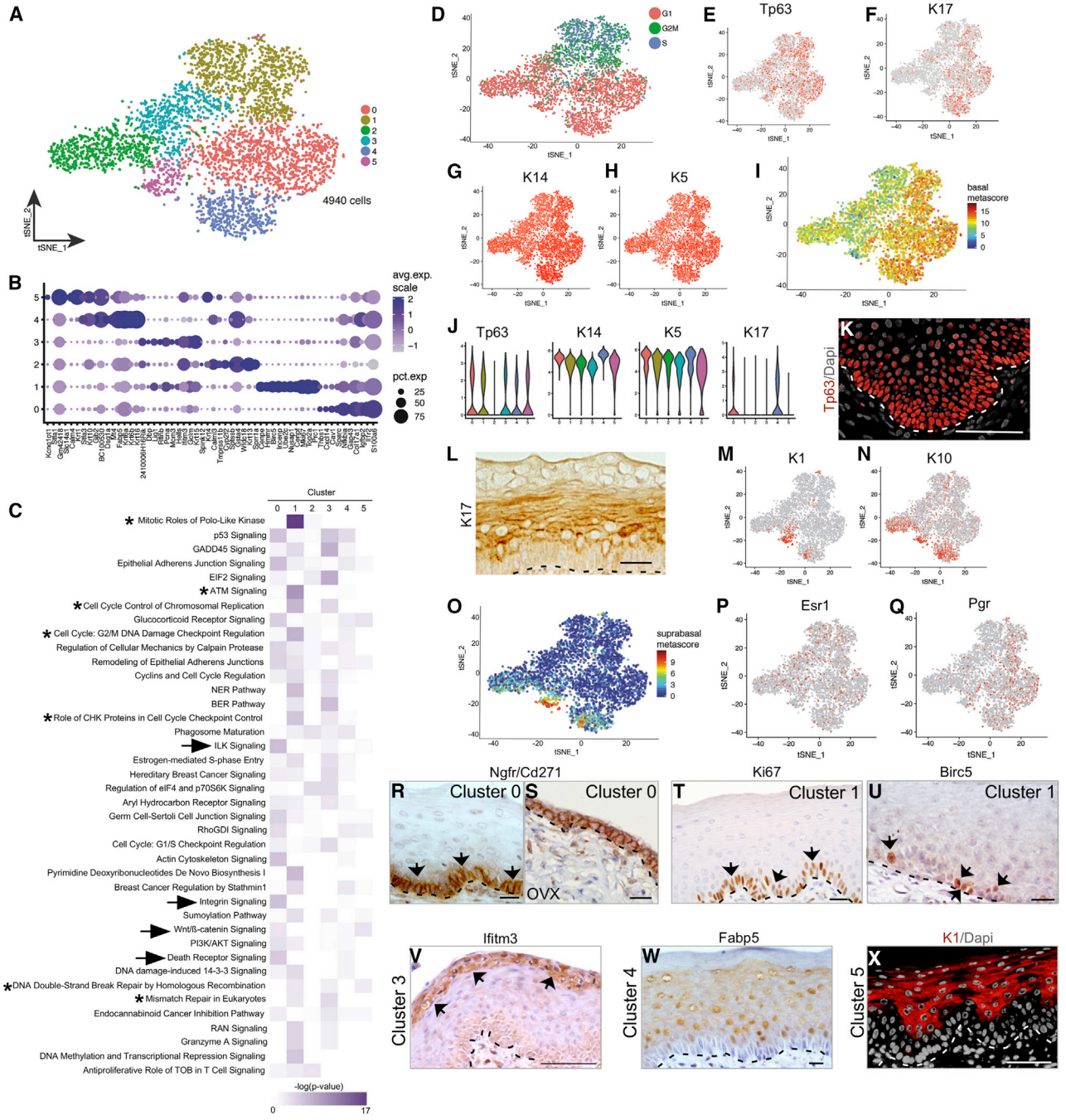


**Figure 1. scRNA-Seq Shows Heterogeneity in VE**

(A) tSNE plot of cell groups defined by k-means clustering analysis in mouse vaginal epithelium (VE).

(B) Dot plot shows the expression of top differential genes and their level of expression in different clusters identified.

(C) IPA analysis showing the upregulation of different canonical pathways in relation to the clusters.

(D) tSNE plot showing cell groups in each cell-cycle phase per cluster.

(E–I) tSNE plot showing expression of *Tp63* (E), *K17* (F), *K14* (G), *K5* (H), and a basal cell signature (I).

(J) Violin plots showing *Tp63*, *K14*, *K5*, and *K17* expression in each cell cluster.

(K and L) Immunostaining for Tp63 (K) and K17 (L) in mouse VE.

(M–Q) tSNE plots showing expression of *K1* (M), *K10* (N), a suprabasal signature (O), *Esr1* (P), and *Pgr* (Q) in different cell clusters.

(R–X) Immunostaining of vaginae for Ngfr/Cd271 (R and S) corresponding to cluster 0, Ki67 (T) and Birc5 (U) corresponding to cluster 1, Ifitm3 (V) corresponding to cluster 3, Fabp5 (W) corresponding to cluster 4, and K1 (X) corresponding to cluster 5. The dotted line demarcates epithelium from adjoining stroma.

Arrows and asterisk in (C) point to stem/progenitor cell-related pathways and cell-cycle-associated pathways, respectively. Arrows in (R–V) mark positive cells. OVX, ovariectomized, L, lumen, S, stroma. Bar, 100 μm.

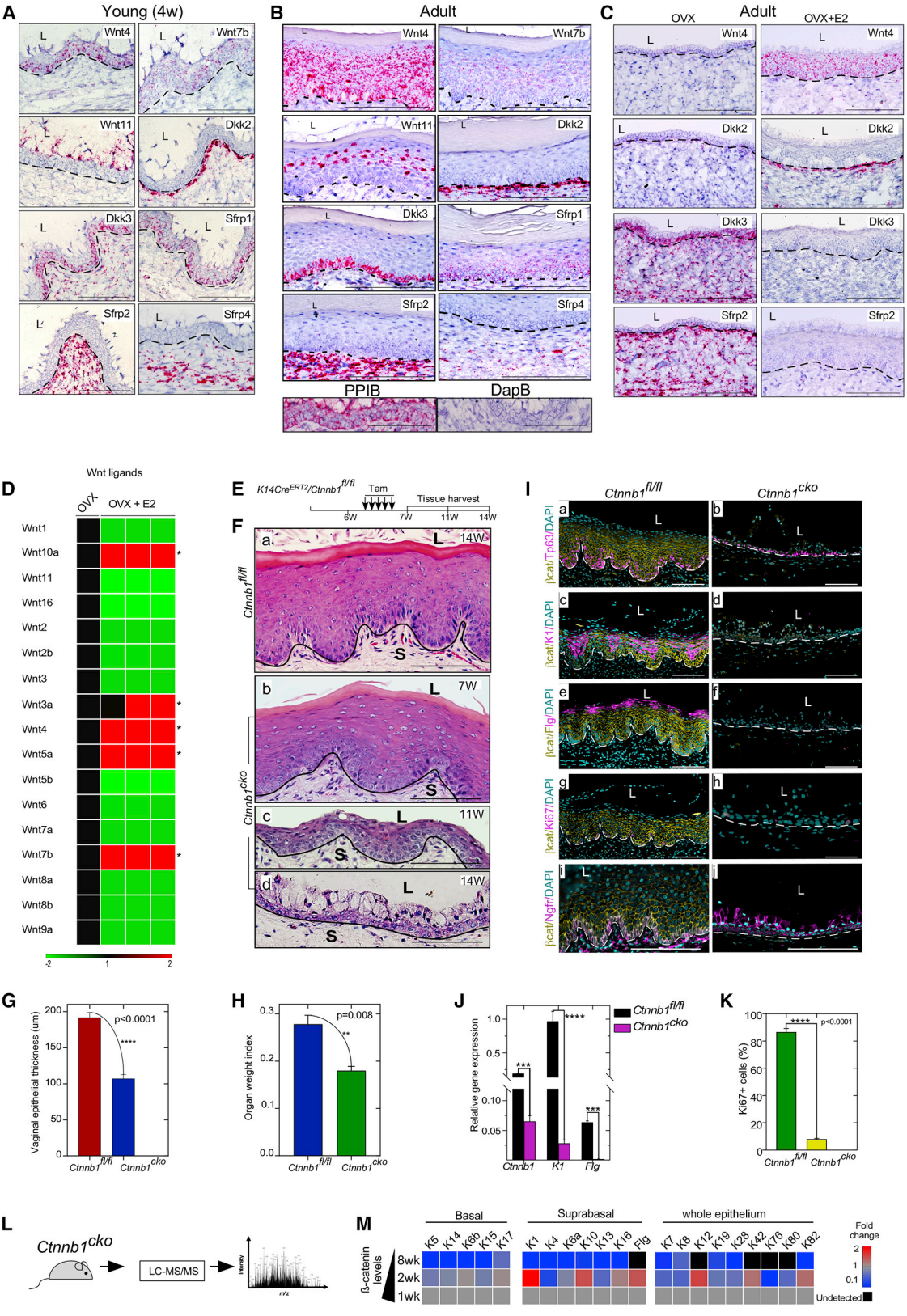


*(legend on next page)*

and various stages of epithelial differentiation as suggested by the expression of markers including K13 (keratin 13), Calml3 (calmodulin-like protein 3), K4, and Ifitm3 (interferon-inducible transmembrane protein 3) (Figures 1B and 1C; Table S1). Finally, clusters 4 and 5, expressing K1 and K10, represented terminally differentiated cells (Figures 1A–1C).

Next, we examined the expression of some of the well-established markers of basal (Tp63, K17, K14, and K5) and suprabasal/cornified cells (K1 and K10) of adult VE (Gimenez-Conti et al., 1994; Kurita et al., 2005). The basal cell markers were broadly expressed in almost all of the cell clusters, marking both proliferating and differentiating cells (Figures 1E–1J). Immunostaining for Tp63 and K17 also confirmed that their expression is present in both the basal and suprabasal layers and is not limited to a specific basal layer (Figures 1K and 1L). Expression of K1 and K10 validated that clusters 2, 4, and 5 consist of differentiated cells (Figures 1M and 1N), which was further confirmed by scoring for the gene signature of suprabasal cells (Figure 1O). Consistent with the *in situ* expression of estrogen and progesterone receptors (Esr1 and Pr) in mouse VE (Li et al., 2018; Mehta et al., 2016), their expression was widely present in all clusters (Figures 1P and 1Q). Using immunohistochemistry, we validated the expression of some of these newly discovered markers representing the different cell clusters to confirm whether they are bona fide markers of specific subsets of VE cells. In both normal and atrophied VE, Ngfr/Cd271 (nerve growth factor receptor), a member of the death receptor signaling family and an established marker of the lung stem cells (Lavrik et al., 2005; Rock et al., 2009), was mainly expressed in a single layer of basal cells located adjacent to stroma (Figures 1R and 1S). This single layer of basal cells, along with cluster 1, also expressed Ki67 (Figure 1T). Birc5, a specific marker of the G2/M phase of the cell cycle (Caldas et al., 2005), was also expressed by the same basal layer, although the expression was limited to fewer cells compared to Ki67 (Figure 1U). Given that the Ki67 expression is maintained in post-mitotic cells that have already exited the cell cycle (Pacal and Bremner, 2012; Sobecki et al., 2017), we concluded that only a few cells in the basal layer are actively proliferating, as marked by Birc5. Ifitm3, a known inhibitor of Zika virus replication (Savidis et al., 2016), marked a unique subset of suprabasal cells (Figure 1V), suggesting that these cells might be involved in the antiviral defense of VE. Fab5 (fatty acid binding protein 5) and K1 expression was present in the majority of the suprabasal cells but the expression was absent in the single basal cell layer ($Ngfr^{+}$ $Ki67^{+}$) adjacent to the stroma (Figures 1W and 1X), implying their status as differentiating cells. We further analyzed some of the markers of these different cell clusters in the human protein atlas database and identified a similar level of heterogeneity in human VE (Figures 1B and S1). In summary, these data highlight the heterogeneity in the basal and suprabasal layers of VE. We also discovered new bona fide markers of different subpopulations of VE cells.

## Mapping Wnt Signaling Changes in Normal and Regenerated VE

Given that Wnt/β-catenin signaling was one of the most enriched pathways in the VE cells (Figure 1C), we looked at the expression of various Wnt pathway members in mouse vagina including Wnt ligands, secreted frizzled-related protein genes (*Sfrp1–5*), Dickkopf-related protein 1–4 (*Dkk1–4*), and WNT inhibitory factor 1 (*Wif1*) using RNA *in situ* hybridization. In young mice (Figure 2A), *Wnt4* and *Wnt7b* expression was present in both basal and suprabasal layers, whereas *Wnt11* expression was restricted to suprabasal cells. In adulthood (Figure 2B), mice retained the *Wnt4* and *Wnt11* expression pattern of young mice; however, *Wnt7b* expression got mainly restricted to suprabasal layer. In both young and adult vaginae (Figures 2A and 2B), *Dkk2*, a known Wnt inhibitor, was expressed in stromal cells subjacent to the basal layer, whereas *Dkk3* and *Sfrp1* were predominantly expressed in basal cells but not in the suprabasal cells. The expression of *Sfrp2* and *Sfrp4* was exclusive to the vaginal stroma in both young and adult vaginae (Figures 2A and 2B).

E2 treatment alone is sufficient to cause the complete regeneration of atrophic VE in ovariectomized (OVX) mice (Miyagawa and Iguchi, 2015). To determine whether E2 activates Wnt signaling during VE regeneration, we assessed changes in the expression levels of Wnt ligands and Wnt inhibitors/modulators in response to E2 treatment, by performing *in situ* hybridization in atrophied VE of OVX mice and E2-induced regenerated VE (Figure 2C). E2 treatment resulted in the upregulation of *Wnt4* and *Dkk2* expression in the regenerated VE compared to the vehicle-treated atrophied VE (Figure 2C), and the expression was similar to adult cycling vaginae (Figure 2B). In contrast, *Dkk3* and *Sfrp2* expression was downregulated in E2-treated mice compared to the

**Figure 2. Conditional Inactivation of β-Catenin Leads to Defective Self-renewal and Differentiation of Vaginal Epithelial Cells**

(A and B) *Wnt4*, *Wnt7b*, *Wnt11*, *Dkk2*, *Dkk3*, *Sfrp1*, *Sfrp2*, and *Sfrp4* mRNA in pre-pubertal (A) and adult (B) mice VE.

(C) *In situ* hybridization for *Wnt4*, *Dkk2*, *Dkk3*, and *Sfrp2* in OVX and E2-treated OVX VE. The housekeeping gene peptidylprolyl isomerase B (*Ppib*) and the bacterial gene dihydrodipicolinate reductase (*DapB*) were positive and negative controls, respectively.

(D) Expression of Wnt ligands in VE upon E2 treatment of OVX mice compared to vehicle-treated OVX control mice.

(E) Schematic depicting the regimen for induction of recombination in $Ctnnb1^{fl/fl}$ mice.

(F) H&E staining of VE in $Ctnnb1^{fl/fl}$ mice at 14 weeks age (a) and $Ctnnb1^{cko}$ mice at 7 (b), 11 (c), and 14 (d) weeks age.

(G and H) Quantification of vaginal epithelial thickness (G) ($n = 3$, $p < 0.0001$) and organ weight index (H) ($n = 3$, $p = 0.008$) in control and $Ctnnb1^{cko}$ mice.

(I) Co-immunostaining for β-catenin with Tp63 (a basal cell marker; a and b), K1 (a stratified squamous epithelium differentiation marker; c and d), filaggrin (Flg; a terminal epithelial cell differentiation marker; e and f), Ki67 (a marker of cell proliferation, g and h), and Ngfr (a marker of stem cells, i and j) in control and $Ctnnb1^{cko}$ mice VE.

(J) Relative levels of *Ctnnb1* (β-catenin), *K1*, and *Flg* in control and $Ctnnb1^{cko}$ mice ($n = 3$).

(K) Quantification of $Ki67^{+}$ cells in control and $Ctnnb1^{cko}$ mice VE ($n = 3$, $p < 0.0001$).

(L) Schematic depicting VE specific β-catenin deletion and subsequent mass spectrometry analysis.

(M) Heatmap depicts the protein expression pattern of various keratins and Flg identified 1, 2, and 8 weeks after β-catenin deletion.

Data represents mean ± SEM. OVX, ovariectomized, L, lumen. Bar, 100 μm.

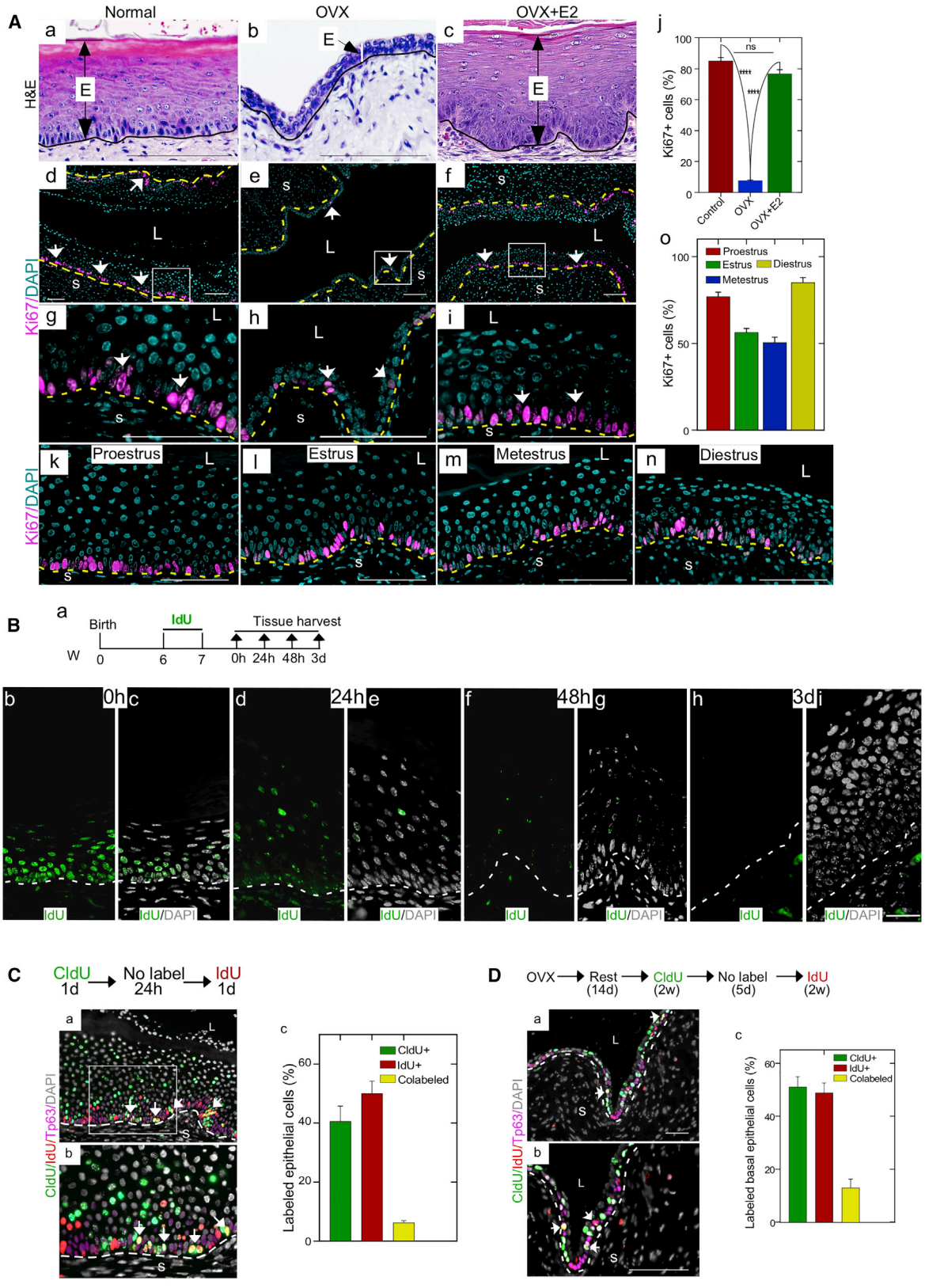


*(legend on next page)*

controls (Figure 2C). For further confirmation of these findings, we performed qPCR arrays to examine the expression of various Wnt ligands (Figure 2D). Expectedly, the expression of several Wnt ligands (*Wnt3a*, *Wnt4*, *Wnt5a*, *Wnt7b*, and *Wnt10a*) was increased in E2-treated group compared to controls (Figure 2D). Collectively, these data suggest that E2-mediated activation of Wnt signaling is finely calibrated by the differential regulation of the expression of various Wnt signaling pathway activators and inhibitors.

### Canonical Wnt/β-Catenin Signaling Is Essential for Vaginal Epithelial Cell Proliferation and Differentiation

To investigate the role of Wnt signaling in VE, we developed a mouse model in which β-catenin (*Ctnnb1*) is specifically ablated in *K14*-expressing cells using a *K14* promoter-driven inducible Cre recombinase (*K14Cre$^{ERT2}$/Ctnnb1$^{fl/fl}$*; *Ctnnb1$^{fl/fl}$*). Administration of a low dose of tamoxifen (1 mg/mouse) for 5 consecutive days to *Ctnnb1$^{fl/fl}$* mice resulted in the recombination of flox *Ctnnb1* alleles in the majority of K14$^+$ cells (*K14Cre$^{ERT2}$/Ctnnb1$^{Δ/Δ}$*; *Ctnnb1$^{cko}$*) (Figure 2E). Histological examination revealed a progressive decrease in VE thickness and the loss of suprabasal layer but not the basal layer in mutants compared to controls (Figure 2F). At 14 weeks of age (7 weeks post-tamoxifen administration), mutant VE consisted of only basal epithelium, which was 1–2 cell layers thick (Figures 2F and 2G). Compared to controls, mutant vaginal organ weight index was also significantly reduced (Figures 2H). As expected, β-catenin protein expression was absent in mutant but not in control epithelium (Figure 2I). To precisely determine the role of Wnt/β-catenin signaling in VE proliferation and differentiation, we performed immunostaining for the markers specific to different VE cell types. Tp63 was expressed by vaginal basal cells in both control and mutant mice (Figures 2Ia and 2Ib). The expression of K1 and filaggrin (Flg), known markers of differentiated VE cells, was present in controls but not in mutants (Figures 2Ic–2If and 2J). Proliferating cells, as marked by Ki67, were present in both controls and in mutants, albeit at a significantly reduced level in the mutant VE (Figures 2Ig, 2Ih, and 2K). Ngfr was also expressed in both control and mutant vaginae (Figures 2Ii and 2Ij). We also performed unbiased quantification of various keratins in mutant VE at different chases post-tamoxifen administration using mass spectrometry. Consistent with our marker analysis, we found a reduction in the expression levels of keratins in the vaginal basal and suprabasal epithelial layers (Figures 2L and 2M). Collectively, these data suggest that canonical Wnt/β-catenin signaling is essential for the proliferation as well as the differentiation of vaginal basal cells.

### VE Self-renews during Regeneration and Normal Growth

In adult mice, VE is a multilayered, stratified, and keratinized epithelium (Figure 3Aa). Ovariectomy-induced E2 withdrawal resulted in the atrophy of VE, which consisted of only 2–3 layers of basal cells (Figure 3Ab). Interestingly, external supplementation of E2 was sufficient to cause the complete regeneration of multilayered stratified squamous VE, which resembled VE of adult cycling mice with intact ovaries (Figures 3Aa–3Ac). When we looked at the expression of Ki67 in the VE of normal cycling mice, atrophied epithelium of OVX mice and the regenerated epithelium of E2-treated OVX mice, it was present mainly in the basal layer adjacent to the basement membrane (Figures 3Ad–3Ai). E2 treatment, however, significantly increased the proliferation index of basal cells in the regenerated epithelium and reinstated it to control levels (Figures 3Ag–3Aj). Since the basal cells proliferate even in absence of ovarian hormones in OVX mice (Figures 3Ah and 3Aj), it seems plausible that E2 is not required for their self-renewal and maintenance. However, E2 is essential for the epithelial regeneration since it increases the proliferation of basal cells (Figures 3Ai and 3Aj), the progenies of which might subsequently differentiate into suprabasal cells. In adult cycling mice, the proliferation was restricted to the basal layer across all cycle stages (Figures 3Bk–3Bo). These results suggest that mitotically active cells are limited to the basal layer of VE that could be the possible site for vaginal stem/progenitor cells.

Next, to define the proliferative compartment of VE, we used an unbiased DNA analog-based technique. This well-established approach has been used successfully to define the proliferative compartments in various other organ systems (Teta et al., 2007). Using the standard protocol (Tuttle et al., 2010), first, we confirmed the specificity of the two different forms of anti-bromodeoxyuridine (BrdU) antisera in detecting the two thymidine analogs, 5-chloro-2-deoxyuridine (CldU) and 5-iodo-2-deoxyuridine (IdU), and the ability of this methodology to detect a well-established intestinal stem cell compartment (Figure S2). To investigate whether VE harbors a label-retaining cell population, we continuously administered IdU to adult cycling mice for 1 week (Figure 3Ba). Analysis of the VE immediately post-IdU administration revealed the presence of IdU-labeled cells mainly in the basal layer (Figures 3Bb and 3Bc), suggesting that the cells had undergone replication during this labeling period. At subsequent chase points, there was a progressive dilution of the IdU

**Figure 3. Proliferating Cells Are Located in the Basal Compartment of Mouse Vagina**

(A) H&E and Ki67 immunostaining of VE from normal cycling mice (a, d, and g), OVX mice (b, e, and h), E2-treated OVX mice (c, f, and i), and adult cycling mice across different estrus-cycle stages (k–n). (g–i) represents high-magnification images of insets in (d)–(f). E in (a)–(c) denotes the thickness of VE. Arrows denote Ki67$^+$ cells. Quantification of Ki67$^+$ cells in VE of mice from the indicated groups (j, n = 3, p = 0.0001) and across estrus-cycle stages (o) is shown.

(B) Schematic of the timeline of IdU administration and subsequent tissue collection (a). Immunostaining for IdU in VE at 0 h (b and c), 24 h (d and e), 48 h (f and g), and 3 days (h and i) post-initial labeling.

(C) Short-term sequential labeling regimen; CldU, IdU, and Tp63 co-staining (a and b); and quantification of CldU$^+$, IdU$^+$, and colabeled cells (c) in mice VE collected 24 h post-IdU treatment.

(D) Long-term sequential labeling regimen in OVX mice; CldU, IdU, and Tp63 co-staining (a and b); and quantification of CldU$^+$, IdU$^+$, and colabeled cells (c) in mice VE collected 24 h post-IdU treatment.

Data represents mean ± SEM. Arrows in (Ca and Cb) and (Da and Db) point toward the cells that are positive for all three markers. The dotted line demarcates epithelium from the adjoining stroma. OVX, ovariectomized, L, lumen, S, stroma. Bar, 100 μm.

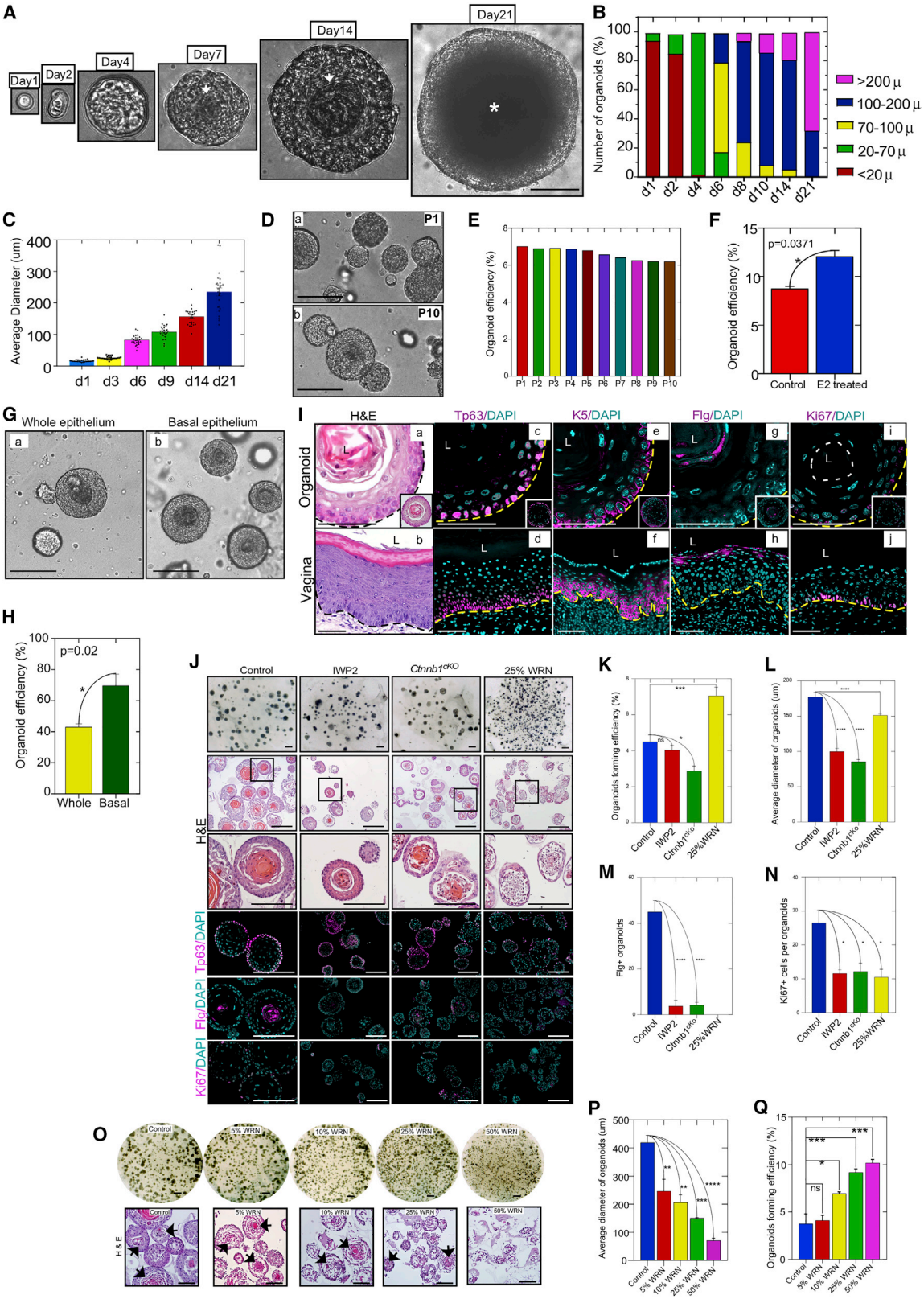


*(legend on next page)*

label in the basal cells (Figures 3Bd–3Bi). By 3 days post-labeling, the IdU label had diluted to below the detection threshold such that none of the basal cells were labeled (Figures 3Bh and 3Bi). This suggested that the IdU-labeled basal cells had undergone multiple rounds of cell division and that there are no slow cycling cells residing in the VE basal compartment. Interestingly, concomitant with the IdU-label dilution in the basal layer, we observed the appearance of IdU-labeled cells in the suprabasal layers (Figures 3Bd–3Bg). These IdU-labeled cells in suprabasal layers correspond to the post-mitotic progenies of labeled basal cells that had left the basal compartment and committed to the differentiation into suprabasal cells. This is consistent with our observation that $Ki67^+$ proliferating cells are also primarily present in the basal layer (Figure 3A).

To determine whether proliferating cells in VE undergo multiple rounds of cell division, we sequentially labeled adult mice with CldU followed by IdU (Figures 3C and S2). Twenty-four hours post-IdU administration, the cells that had undergone cell division during the first round of labeling when CldU was given had differentiated and migrated toward the lumen, while the cells that had undergone cell division during the second round of labeling when IdU was given were mainly confined to the basal cell layers (Figures 3Ca–3Cc). Moreover, the cells that were co-labeled with both CldU and IdU were mainly localized to the basal compartment and were positive for a known basal cell marker Tp63 (Figures 3Ca–3Cc and S2), suggesting that basal cells have the ability to undergo multiple rounds of cell division. Importantly, when we sequentially labeled OVX adult mice with CldU followed IdU (Figure 3D), and analyzed the vaginae 24 h post-IdU labeling, we detected $IdU^+$, $CldU^+$, as well as CldU-IdU co-positive cells in the basal layer of the atrophied VE (Figures 3Da–3Dc), suggesting that the basal cells undergo multiple rounds of cell division even in the absence of ovarian hormones. In summary, these results confirmed that mitotically active proliferating cells are present in the basal layer of VE.

## Establishment and Characterization of Vaginal Organoids

Organoid formation in other organ systems is associated with the presence of adult stem cells (Clevers, 2016). Therefore, to establish the presence of stem/progenitor cells in vagina, we sought to develop vaginal organoids. Briefly, VE was isolated and digested enzymatically into a single-cell suspension of VE cells, which were subsequently cultured in basement membrane matrix extract (BME) supplemented with epidermal growth factor (EGF), a TGF-βr kinase inhibitor (transforming growth factor β receptor), and a ROCK inhibitor (Rho-associated protein kinase). In comparison to the complex culture conditions and media composition used in the organoid culture of various other organs (Kaushik et al., 2018), our relatively simple culture conditions were sufficient for these single cells to develop into organoids when cultured for 21 days (Figure 4A). Importantly, these vaginal organoids developed from single cells and progressively grew in size (Figures 4A–4C). By 7 days, a differentiated suprabasal cell layer was formed in the center of the organoids (Figures 4A–4C, arrow). At 21 days of culture, the lumen was filled with mucinous secretions (Figure 4A, asterisk), which is a natural characteristic of the VE *in vivo* (Carson et al., 1998). A cardinal feature of stem cell-derived organoids is their ability to propagate in culture conditions for a long time (Clevers, 2016). Accordingly, these vaginal organoids could also be maintained for a long time through serial passaging (Figures 4D and 4E). Expectedly, treatment with E2 increased the growth of these organoids (Figure 4F). To determine whether the basal cells are more efficient in developing organoids, we cultured isolated VE cells from OVX mice. We found that the organoid forming efficiency of basal cells was significantly higher compared to the whole VE (Figures 4G and 4H).

Histological examination revealed that these vaginal organoids comprising multilayered epithelial cells organized into basal and suprabasal layers with a keratinized center, which is similar to *in vivo* mouse VE (Figures 4Ia and 4Ib). The expression pattern of the known basal cell (Tp63 and K5) and suprabasal/keratinized cell (Flg) markers was also comparable to *in vivo* vaginal tissue (Figures 4Ic–4Ih). As expected, proliferating cells ($Ki67^+$) were mainly restricted to the basal layer in both the organoids as well as mouse vagina (Figures 4Ii and 4Ij). Importantly, these organoids survive freeze-thaw cycles such that they can be frozen in liquid nitrogen and thawed for subsequent culturing at later dates. In summary, we have established a simple and

**Figure 4. Establishment and Characterization of Mouse Vaginal Organoids**

(A) Timeline depicting organoid development from a single mouse vaginal epithelial cell. The arrow and asterisk in (A) indicate the formation of lumen and the accumulation of mucinous secretion respectively.

(B) Quantification of the distribution of organoid sizes over a period of 21 days in culture.

(C) Quantification of the average organoid size at various days of culture.

(D and E) Representative images (Da and Db) and quantification (E) of the organoid formation efficiency at indicated passages.

(F) Organoid formation after estrogen treatment (n = 5 mice; p = 0.0371).

(G and H) Representative images of the organoids (Ga and Gb) and quantification of the organoid formation efficiency (H) of cells isolated from the whole epithelium and the basal epithelium (n = 3, p = 0.02).

(I) Histological analysis (a and b) and immunostaining for Tp63 (c and d), K5 (e and f), filaggrin (g and h), and Ki67 (i and j) of mouse vaginal organoids and *in vivo* VE.

(J) Histological analysis and immunostaining for Tp63, filaggrin, and Ki67 of vaginal organoids cultured in presence of vehicle (control), IWP2, and 25% WRN or those developed from epithelial cells isolated from $Ctnnb1^{fl/fl}$ mice and cultured in presence of tamoxifen ($Ctnnb1^{cko}$).

(K and L) Quantification of organoid forming efficiency (K) and organoid size (L) in indicated treatment groups (n = 5 mice, *p < 0.05, ***p < 0.001, ****p < 0.0001).

(M and N) Quantification of filaggrin positive organoids (M) and the average number of $Ki67^+$ cells per organoid (N) in the indicated treatment groups (n = 5, *p < 0.05, ****p < 0.0001).

(O Representative images and histology of organoids cultured in presence of the indicated concentrations of WRN-conditoned medium.

(P and Q) Quantification of the organoid size (P) and organoid formation efficiency (Q) at indicated concentrations of WRN-conditioned medium (n = 5 mice, *p < 0.05, ***p < 0.001, ****p < 0.0001).

Data represents mean ± SEM. Arrows mark differentiated cells. L, lumen, p, passage. Bar, 100 μm.

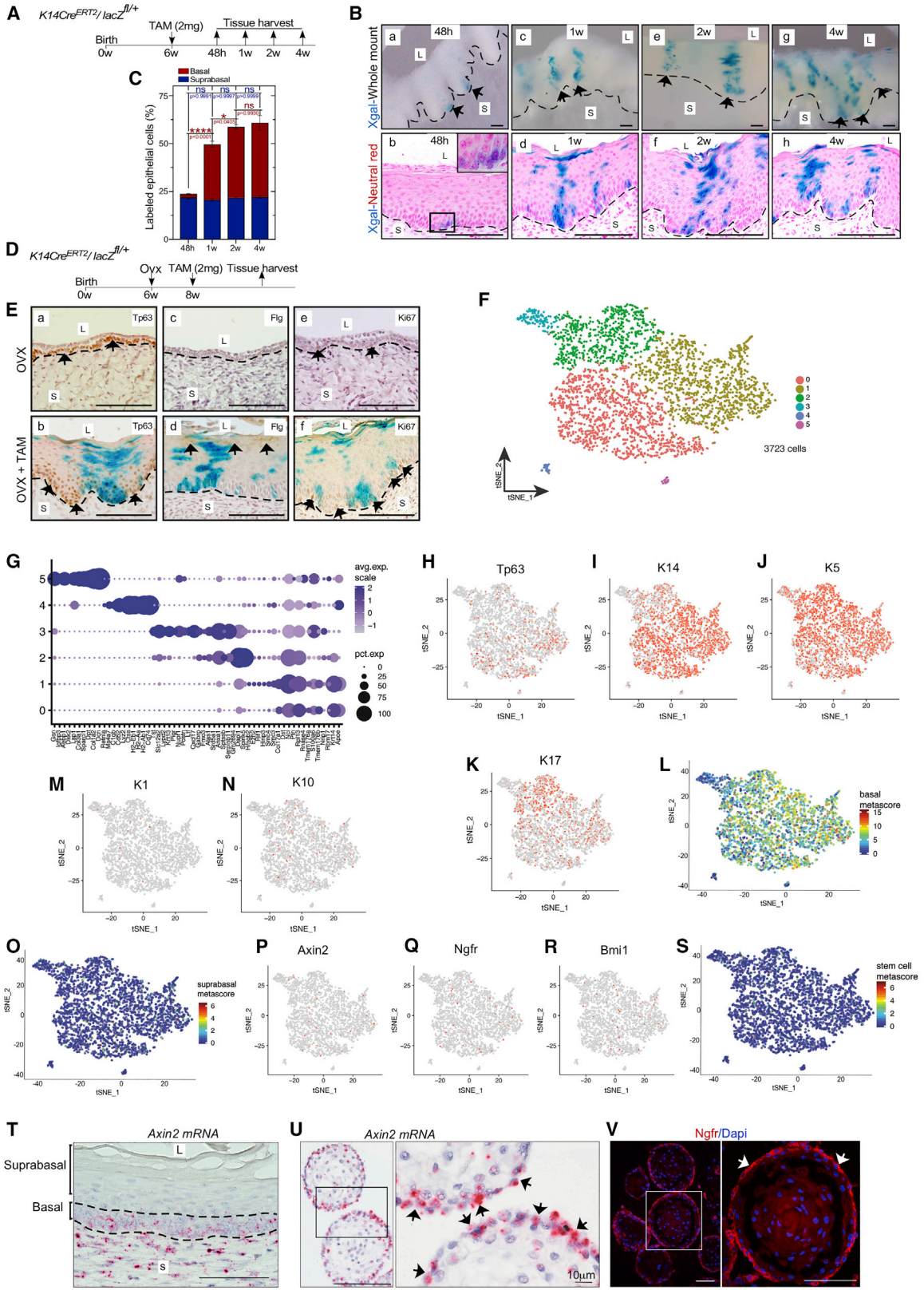


*(legend on next page)*

highly efficient method of developing vaginal organoids, which closely mimic the mouse VE.

To investigate further the role of Wnt signaling in VE maintenance, we examined the response of vaginal organoids to Wnt signaling modulation (Figure 4J). Treatment with IWP-2, a proven small-molecule inhibitor of Wnt signaling (Chen et al., 2009), decreased the number and size of organoids (Figures 4J–4L). A similar phenotype was displayed by the organoids developed from the VE cells isolated from *Ctnnb1*$^{fl/fl}$ mice and treated *in vitro* with a low dose of tamoxifen to induce the ablation of β-catenin (Figures 4J–4L). On the other hand, activation of Wnt signaling by adding WRN (Wnt3a, Rspondin, and Noggin) conditioned media to organoids significantly increased their number but decreased their size as compared to the control organoids (Figures 4J–4L). Histological and marker (Tp63 and Flg) analysis revealed that Tp63$^+$ basal cells were located at the periphery of organoids in all the groups (Figure 4J). However, Flg$^+$ differentiated cells were only present in the control group and were rarely seen in organoids from the other three groups (Figures 4J and 4M). Proliferating cells were present in the basal layer, but their number was decreased in all the groups compared to controls (Figures 4J and 4N). Since, in IWP2, *Ctnnb1*$^{cko}$, and WRN groups, organoids were smaller in size as compared to the control group and were missing the differentiated cell layers, quantifying the percentage of total Ki67$^+$ cells would overestimate the proliferation index of organoids in these groups, which is otherwise lower than the control group. Therefore, we quantified the number of Ki67$^+$ cells per organoid rather than the percentage of Ki67$^+$ cells. Next, we assessed the impact of increasing Wnt signaling on the organoid growth. We found that with a progressive increase in the WRN conditioned medium concentration, the organoid formation efficiency significantly increased (Figures 4O–4Q). However, organoids cultured in high Wnt (50% WRN) conditions were smaller in size and lacked a typical differentiated cell layer normally present in the center of the vaginal organoids (Figures 4O and 4Q), implying that hyperactive Wnt signaling impairs both the proliferation and differentiation of vaginal basal cells. In summary, these results suggest that balanced Wnt signaling is essential for the proliferation and differentiation of vaginal basal epithelium.

### *In Vivo* Genetic Cell Lineage Tracing of K14$^+$ Basal Cells

Given that the cell proliferation is limited to basal cells, which are more efficient in forming organoids containing all VE cell types (Figures 3 and 4), next, we decided to trace the fate of K14$^+$ basal cells and determine their contribution to other cell lineages of VE. For that, we performed genetic cell lineage tracing using *K14Cre*$^{ERT2}$/*lacZ*$^{fl/+}$ *(K14lacZ)* mice, in which *K14Cre* recombinase-expressing cells and their descendants express *lacZ* upon tamoxifen administration (Figures 5A–5C). Previous cell-fate tracing studies have identified *K14Cre*-marked basal cells as the stem cells of lung (Hong et al., 2004), bladder (Papafotiou et al., 2016), and prostate (Ousset et al., 2012). Compared to the widespread *in situ* expression of K14, *K14Cre* is expressed in fewer cells, allowing for clonal analysis of marked cells, especially after a low dose of tamoxifen administration (Figures 1G, 5A, and 5B). Therefore, we labeled the K14$^+$ cells of adult VE by administering *K14lacZ* mice with a single dose of tamoxifen (2 mg/mouse) (Figure 5A). Forty-eight hours after the tamoxifen injection, single cells at the base of the VE were marked with *lacZ*, as is indicated by the blue labels in (Figure 5Ba, arrow). At subsequent chase points, these LacZ-labeled K14$^+$ cells and their progenies populated the entire VE, which was evident as parallel strips of lacZ$^+$ cells originating from the base and progressing through the suprabasal layer toward the lumen (Figures 5B and 5C). Expectedly, *K14lacZ* mice without tamoxifen exposure showed no lacZ activity (Figure S3). These results suggest that K14$^+$ basal cells can self-renew and give rise to the suprabasal cells of VE.

To investigate whether basal cells are involved in VE regeneration, we traced the fate of labeled K14$^+$ basal cells during tamoxifen induced VE regeneration. For that, we OVX *K14lacZ* females to induce atrophy of VE (Figure 5D). Expectedly, after a rest period of 14 days necessary to get rid of the remaining circulating ovarian hormones, the atrophied VE of these mice comprised of a thin epithelial layer, which consisted mainly of basal cells (Tp63$^+$ and Flg$^-$) (Figures 5Ea and 5Ec). Next, we injected these OVX *K14lacZ* mice with a single dose of tamoxifen (2 mg/mouse; Figure 5D), which serves two distinct functions in this model system. First, it activates the *K14Cre* recombinase to cause the recombination of flox lacZ alleles. Second, due to its strong pro-estrogenic activity, it causes the regeneration of VE, similar to what we observed after E2 supplementation (Figure 3B). Indeed, the atrophied VE of OVX *K14lacZ* mice completely regenerated following the tamoxifen administration. Importantly, the newly regenerated suprabasal layer was LacZ labeled (Figures 5Eb, 5Ed, and 5Ef). Both Tp63$^+$ and Flg$^+$ cells were present in the lacZ$^+$ epithelial streaks, confirming the

**Figure 5. Vaginal Basal Cells Contribute to Epithelial Renewal during Normal Growth and Regeneration**

(A) Schematic depicting label induction in *K14Cre*$^{ERT2}$/*lacZ*$^{fl/+}$ mice.

(B and C) X-gal staining of *K14Cre*$^{ERT2}$/*lacZ*$^{fl/+}$ mice vaginae (B) and quantification of labeling index (C) at 48 h (a and b), 1 week (c and d), 2 weeks (e and f), and 4 weeks (g and h) post-induction (n = 3, *p < 0.05, ****p < 0.0001). Arrows indicate βgal$^+$ vaginal epithelial cells.

(D) Schematic depicting label induction in OVX *K14Cre*$^{ERT2}$/*lacZ*$^{fl/+}$ mice.

(E) Xgal staining and immunostaining for Tp63 (a and b), filaggrin (c and d), and Ki67 (e and f) in vaginae of vehicle (a, c, and e) and tamoxifen (b, d, and f)-treated OVX *K14Cre*$^{ERT2}$/*lacZ*$^{fl/+}$ mice.

(F) A tSNE plot of cell clusters defined by k-means clustering analysis in atrophied VE of OVX mice.

(G) Dot plot showing the expression level of differential genes in each of the clusters identified.

(H–S) tSNE plots showing expression of *Tp63* (H), *K14* (I), *K5* (J), *K17* (K), a basal signature (L), *K1* (M), *K10* (N), a suprabasal signature (O), *Axin2* (P), *Ngfr* (Q), *Bmi1* (R), and a stem cell signature (S).

(T and U) *In situ* hybridization for *Axin2* mRNA in mouse vagina (T) and vaginal organoids (U).

(V) Immunostaining for Ngfr in mouse vaginal organoids.

Data represents mean ± SEM. Dotted lines in (B) and (E) demarcate VE from the adjoining stroma. Dotted lines in (T) demarcate basal epithelium. Black (U) and white (V) arrows point to Axin2$^+$ and Ngfr$^+$ cells, respectively. OVX, ovariectomized, L, lumen, S, stroma, TAM, tamoxifen. Bar, 100 μm unless otherwise indicated.

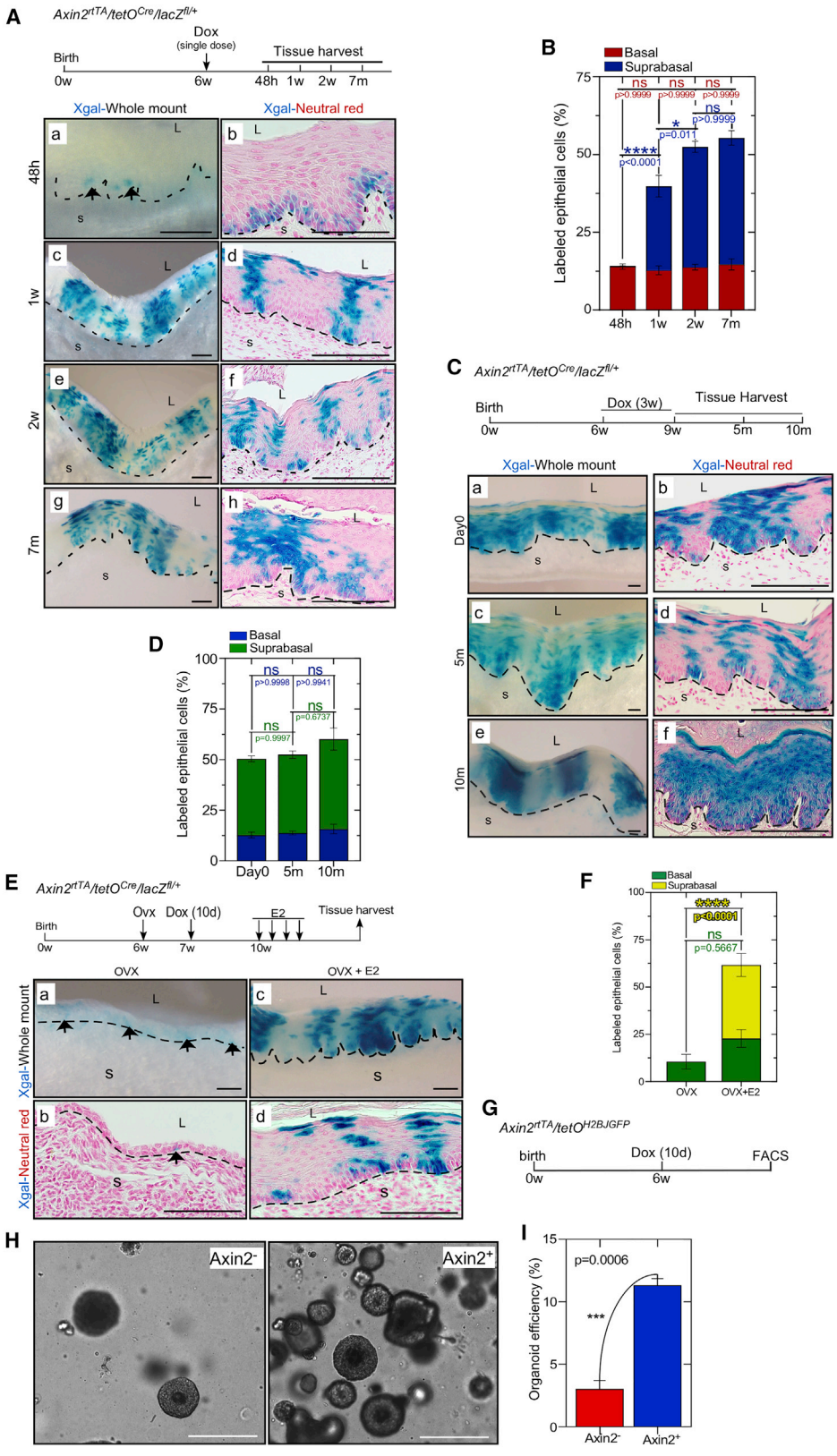


*(legend on next page)*

presence of both basal and suprabasal/keratinized cells in the regenerated epithelium (Figures 5Eb and 5Ed, arrow). Proliferating cells were present at the base of the lacZ$^+$ epithelial streaks, and, comparatively, very few proliferating cells were present in the VE of OVX mice that were not administered with tamoxifen (Figures 5Ee and 5Ef, arrow). This suggests that the actively dividing basal cells drive the regeneration of VE.

## Vaginal Basal Cell Heterogeneity and a Fraction of Cells Marked by Stem Cell-Related Markers

To understand the basal cell heterogeneity and identify the signaling pathways that are involved in the maintenance of these cells, we performed scRNA-seq analysis of the OVX epithelium similar to that shown in Figure 1 and compared it with WT epithelium (Figures 5 and S4). A total of 3,723 cells that passed the QC filter were analyzed (Figure 5F; Table S1). Using k-means method these cells were categorized into 6 cell clusters (0–5), which were visualized using tSNE projection (Figure 5F). Interestingly, marker expression of clusters 0, 1, and 2 was consistent with that of basal cells (K14$^+$, Tp63$^+$, K5$^+$, K17$^+$, and positive for a basal signature), as was expected from the OVX epithelium (Figures 5G–5L). Furthermore, consistent with our observation in the hormonally intact epithelium (Figure 1), the cells in these clusters also expressed Col17a1, a known marker of skin stem cells (Tanimura et al., 2011), and showed upregulation of Wnt/β-catenin signaling (Figures 5G and S5). Cluster 3 expressed genes involved in epithelial differentiation (Spink5 and K13) (Figures 5F and 5G). Expectedly, we did not observe any defined expression of known markers of differentiated VE cells (K1$^+$, K10$^+$, and a suprabasal signature) (Figures 5M––5O). These data suggest that OVX epithelial cells do not undergo the process of complete differentiation due to lack of estrogen, which is essential for the differentiation of this epithelium (Miyagawa and Iguchi, 2015), although some of the cells are committed for early differentiation as reflected by their expression of Spink5 and K13. Due to a low cell number and a high percentage of mitochondrial genes and the genes associated with immune system, we did not consider clusters 4 and 5 for further analysis (Figures 5F and 5G). Given the highly regenerative nature of OVX VE cells, next, we examined the expression of some of the known markers of stem/progenitor cells of various other organ systems (Table S1). Interestingly, these OVX VE cells did express some of the known stem cell markers (Axin2, Ngfr, Bmi1, and a signature of stem cells), albeit at a lower level (Figures 5P–5S). We confirmed the expression of *Axin2* mRNA using *in situ* hybridization-based analysis of adult VE as well as vaginal organoids, which revealed that the expression was indeed limited to a single layer of basal cells (Figures 5T and 5U). The relatively higher expression of *Axin2* revealed by *in situ* hybridization-based analysis compared to scRNA-seq data was expected due to a lower efficiency (~10% per molecule) of mRNA detection in droplet scRNA-seq method (Salomon et al., 2019). Similar to *Axin2* mRNA, the expression of Ngfr was also limited to a single layer of basal cells in vaginal organoids (Figure 5V).

So far, our results suggest that vaginal basal cells, which survive hormonal deprivation, harbor a population of highly proliferative cells, presumably vaginal stem cells, that are capable of completely regenerating the entire VE upon E2 stimulation (Figure 3). Interestingly, E2-mediated regeneration is finely calibrated by differential expression of Wnt signaling pathway members (Figure 2). Moreover, clusters 0 in intact epithelium (Figure 1) and 0, 1, and 2 in OVX epithelium (Figure S5), all of which localize to the vaginal basal layer, show significant upregulation in Wnt signaling pathway, which in turn is responsible for the proliferation and differentiation of these cells (Figure 2). Therefore, it seems plausible that VE stem cells, presumably residing in the basal layer, are Wnt-responsive cells. Given that one of the classic Wnt-reporter genes that also faithfully marks Wnt-responsive stem cells in several other regenerative organs is Axin2 (Clevers et al., 2014), and that Axin2 is expressed exclusively by a single layer of vaginal basal cells (Figures 5P and 5T), we decided to trace the fate of Axin2-derived cells to investigate their role as vaginal stem cells

## Cell Lineage Tracing of Axin2$^+$ Cells in VE

To determine the contribution of Axin2$^+$ cells toward VE homeostasis, we permanently labeled Axin2$^+$ cells and followed the fate of their progenies in normally cycling mice (Figure 6A). Therefore, we used doxycycline-inducible *Axin2$^{rtTA}$/tetO$^{Cre}$/lacZ$^{fl/+}$* mice to pulse label Axin2$^+$ cells stochastically with lacZ. Forty-eight hours after the administration of a single dose of doxycycline (2 mg), we found lacZ-labeled cells exclusively in the basal layer

**Figure 6. Axin2 Marks Self-renewing Basal Cells that Can Regenerate the Entire VE**

(A) Schematic depicting the timeline of doxycycline administration for single-cell labeling and subsequent tissue collection. X-gal staining of thick vaginal slices and tissue sections at 48 h (a and b; arrowheads mark βgal$^+$ cells), 1 week (c and d), 2 weeks (e and f), and 7 months (g and h) post-induction.

(B) Quantification of labeling index at indicated time points (n = 3, *p < 0.05, ****p < 0.0001).

(C) Schematic depicting the timeline of doxycycline administration for labeling at saturation. X-gal staining of thick vaginal slices and tissue sections at 0 days (a and b), 5 months (c and d), 10 months (e and f) post-induction.

(D) Quantification of labeling index at indicated time points (n = 3).

(E) Schematic depicting the timeline of doxycycline administration to OVX mice for labeling at a single-cell density and subsequent hormone treatment and tissue collection. X-gal staining of thick slices and tissue sections of vaginae collected 4 days after vehicle (a and b) or estrogen (E2) (c and d) treatment of OVX mice.

(F) Quantification of labeling index in VE of indicated groups (n = 3, ****p < 0.0001).

(G) Schematic of the timeline of doxycycline administration to *Axin2$^{rtTA}$/tetO$^{H2BJGFP}$* mice and FACS of Axin2$^+$ and Axin2$^-$ cells for *in vitro* 3D culture.

(H) Bright-field images of organoids developed from Axin2$^-$ and Axin2$^+$ cells.

(I) Quantification of organoid forming efficiency of Axin2$^-$ and Axin2$^+$ cells (n = 5 mice; p = 0.0006).

The black dotted line demarcates VE from the adjoining stroma.

Data represents mean ± SEM.

Dox, doxycycline, E2, 17-β-estradiol, OVX, ovariectomized, L, lumen, S, stroma. Bar, 100 μm (500 μm for whole-mount and organoid images).

(Figures 6Aa and 6Ab), which was consistent with *Axin2* mRNA expression (Figure 5). Control mice without doxycycline exposure did not show any lacZ expression (Figure S6). At subsequent chase points, these LacZ-labeled Axin2$^+$ cells expanded, and their progenies populated the entire VE, which was evident as parallel streaks of lacZ$^+$ cells originating from the base and progressing through the suprabasal layer toward the lumen (Figures 6Ac–6Ah and 6B). This suggests that Axin2$^+$ basal cells give rise to all other epithelial cell lineages of VE.

One of the hallmarks of stem cells is their ability to self-renew (Clevers et al., 2014). To investigate whether Axin2$^+$ cells self-renew, we labeled a maximum number of Axin2$^+$ cells in *Axin2*$^{rtTA}$/*tetO*$^{Cre}$/*lacZ*$^{fl/+}$ mice by administering doxycycline at high doses for an extended period of time (3 weeks) (Figure 6C). At 0 days, lacZ$^+$ basal cells and their progenies in the suprabasal layers were present as parallel strips of labeled cells throughout the VE (Figures 6Ca and 6Cb). Even after 10 months of chase, this pattern of lacZ labeling was maintained in the VE. More importantly, the proportion of labeled basal cells remained stable throughout the chase (Figures 6Cc–6Cf and 6D). These data suggest that Axin2$^+$ cells self-renew and are not replaced by unlabeled Axin2$^-$ cells.

Next, we tested the regenerative potential of Axin2$^+$ basal cells. Adult *Axin2*$^{rtTA}$/*tetO*$^{Cre}$/*lacZ*$^{fl/+}$ mice were OVX to induce vaginal epithelial atrophy. After a rest period of 14 days, mice were fed doxycycline-treated water for 10 days (Figure 6E), which resulted in the labeling of a subset of Axin2-expressing basal cells (Figures 6Ea and 6Eb). Expectedly, administration of E2 completely regenerated the VE (Figures 6Ec and 6Ed). Importantly, the singly labeled Axin2$^+$ cells expanded and differentiated into labeled suprabasal cells, repopulating the entire VE as shown by lacZ$^+$ strips of basal cells and their progenies (Figures 6Ec and 6Ed and 6F). These results suggest that Axin2-expressing cells are ovariectomy-resistant Wnt-responsive cells that robustly contribute to VE regeneration upon E2 administration.

To investigate whether organoid forming ability is exclusive to Axin2$^+$ cells, we used fluorescence-activated cell sorting (FACS) to sort Axin2$^+$ and Axin2$^-$ cells from *Axin2*$^{rtTA}$/*tetO*$^{H2BJGFP}$ mice and cultured them to develop organoids (Figure 6G). On an average, 11.33% ± 0.52% of Axin2$^+$ cells formed organoids compared to Axin2$^-$ cells (3.03% ± 0.68%) (Figures 6H and 6I). Thus, organoid forming efficiency of Axin2$^+$ cells is significantly higher than that of Axin2$^-$ cells.

## DISCUSSION

E2 signaling is a master regulator of reproductive tract functions, and its dysregulation leads to many diseases including cancer (Hewitt and Korach, 2018). E2 stimulates the proliferation and differentiation of VE cells (Buchanan et al., 1998). VE cell-specific deletion of estrogen receptor 1 (ESR1) in mice revealed that estrogen signaling is essential for the differentiation but not the proliferation of VE (Li et al., 2018). This is supported by the observations in OVX mice and *in vitro* organ culture studies that epithelial cells are able to proliferate at a baseline level in the absence of E2 signaling (Gimenez-Conti et al., 1994; Tsai and Bern, 1991). Comparative analysis of vaginae from the E2-treated control and ESR1 knockout mice using DNA microarrays showed that 6 out of top 10 most upregulated genes in the control group belong to Wnt signaling pathway (Miyagawa and Iguchi, 2015), suggesting that E2-mediated effects on vagina might occur through Wnt signaling. This is further supported by the findings that diethylstilbestrol treatment in mice affects Wnt signaling and causes persistent upregulation of Wnt4 (Nakamura et al., 2012). Consistently, we showed that treatment of OVX mice with E2 leads to the upregulation of many Wnt ligands and the downstream targets. Our results also demonstrated that, even in the presence of tamoxifen and intact functioning ovaries, basal/stem cells in the VE of *Ctnnb1*$^{cko}$ mice were unable to undergo differentiation to give rise to suprabasal cells. This suggests that canonical Wnt signaling might be a key mediator of E2-induced differentiation of VE cells.

## STAR★METHODS

Detailed methods are provided in the online version of this paper and include the following:

- KEY RESOURCES TABLE
- LEAD CONTACT AND MATERIALS AVAILABILITY
- EXPERIMENTAL MODEL AND SUBJECT DETAILS
  - Mice
  - Epithelial cell isolation and organoid culture
  - Cell lines
- METHOD DETAILS
  - Targeting lacZ expression
  - Histology and immunostaining
  - Beta-galactosidase/X-gal staining
  - CldU-IdU labeling
  - Vaginal epithelial protein isolation and digestion for proteomic analysis
  - Mass spectrometry and database searching
  - *In Situ* Hybridization (ISH)
  - Wnt Signaling qPCR arrays
  - Microscope image acquisition
- QUANTIFICATION AND STATISTICAL ANALYSIS
  - Single Cell RNaseq analysis
  - Statistical Analysis
- DATA AND CODE AVAILABILITY

### SUPPLEMENTAL INFORMATION

Supplemental Information can be found online at https://doi.org/10.1016/j.celrep.2020.01.003.

### ACKNOWLEDGMENTS

We would like to thank Prof Jose Teixeira (Michigan State University) and members of the Tanwar's lab for critical reading and valuable inputs, Dr. Annemiek Beverdam (University of New South Wales) for help with K14cre mice, Jyoti Goad, Varshini D. Venkata, Arnab Ghosh, and Annie Ko for technical assistance, Nicole Cole (Analytical and Biomolecular Research Facility) for FACS sorting, and Rob Salomon (Garvan Institute) for single-cell sequencing. Work in the Tanwar's lab was in part supported by funding from National Health and Medical Research Council, Australian Research Council, and Ovarian Cancer Research Foundation. D.G.-O. is supported by a Cancer Institute NSW Career Development Fellowship (DG00625).

## AUTHOR CONTRIBUTIONS

Conceptualization, A.A., S.M.S., and P.S.T.; Methodology, A.A., S.M.S., M.F.B.J., Y.C.-S., D.G.-O., and P.S.T.; Investigation, A.A., S.M.S., and P.S.T.; Data Collection and Analysis, A.A., S.M.S., M.F.B.J., Y.C.-S., D.G.-O., and P.S.T.; Writing – Review & Editing, A.A., S.M.S., M.F.B.J., Y.C.-S., D.G.-O., and P.S.T.; Funding Acquisition, P.S.T.

## DECLARATION OF INTERESTS

P.S.T. is an inventor on a patent application regarding vaginal organoid culture and its uses. All other authors have no competing interests to declare.

Received: June 13, 2019
Revised: November 1, 2019
Accepted: December 30, 2019
Published: February 4, 2020

## REFERENCES

Bonnans, C., Flacelière, M., Grillet, F., Dantec, C., Desvignes, J.P., Pannequin, J., Severac, D., Dubois, E., Bibeau, F., Escriou, V., et al. (2012). Essential requirement for β-arrestin2 in mouse intestinal tumors with elevated Wnt signaling. Proc. Natl. Acad. Sci. USA *109*, 3047–3052.

Boretto, M., Cox, B., Noben, M., Hendriks, N., Fassbender, A., Roose, H., Amant, F., Timmerman, D., Tomassetti, C., Vanhie, A., et al. (2017). Development of organoids from mouse and human endometrium showing endometrial epithelium physiology and long-term expandability. Development *144*, 1775–1786.

Bragulla, H.H., and Homberger, D.G. (2009). Structure and functions of keratin proteins in simple, stratified, keratinized and cornified epithelia. J. Anat. *214*, 516–559.

Buchanan, D.L., Kurita, T., Taylor, J.A., Lubahn, D.B., Cunha, G.R., and Cooke, P.S. (1998). Role of stromal and epithelial estrogen receptors in vaginal epithelial proliferation, stratification, and cornification. Endocrinology *139*, 4345–4352.

Butler, A., Hoffman, P., Smibert, P., Papalexi, E., and Satija, R. (2018). Integrating single-cell transcriptomic data across different conditions, technologies, and species. Nat. Biotechnol. *36*, 411–420.

Caldas, H., Jiang, Y., Holloway, M.P., Fangusaro, J., Mahotka, C., Conway, E.M., and Altura, R.A. (2005). Survivin splice variants regulate the balance between proliferation and cell death. Oncogene *24*, 1994–2007.

Carson, D.D., DeSouza, M.M., Kardon, R., Zhou, X., Lagow, E., and Julian, J. (1998). Mucin expression and function in the female reproductive tract. Hum. Reprod. Update *4*, 459–464.

Chen, B., Dodge, M.E., Tang, W., Lu, J., Ma, Z., Fan, C.W., Wei, S., Hao, W., Kilgore, J., Williams, N.S., et al. (2009). Small molecule-mediated disruption of Wnt-dependent signaling in tissue regeneration and cancer. Nat. Chem. Biol. *5*, 100–107.

Clevers, H. (2016). Modeling Development and Disease with Organoids. Cell *165*, 1586–1597.

Clevers, H., Loh, K.M., and Nusse, R. (2014). Stem cell signaling. An integral program for tissue renewal and regeneration: Wnt signaling and stem cell control. Science *346*, 1248012.

Edgar, R. (2002). Gene Expression Omnibus: NCBI gene expression and hybridization array data repository. Nucleic Acids Research *30*, 207–210.

Edgren, R.A. (1959). The modification of estrogen-induced changes in rat vaginas with steroids and related agents. Ann. N Y Acad. Sci. *83*, 160–184.

Gardner, W.U. (1959). Sensitivity of the vagina to estrogen: genetic and transmitted differences. Ann. N Y Acad. Sci. *83*, 145–159.

Ghosh, A., Syed, S.M., and Tanwar, P.S. (2017). *In vivo* genetic cell lineage tracing reveals that oviductal secretory cells self-renew and give rise to ciliated cells. Development *144*, 3031–3041.

Gimenez-Conti, I.B., Lynch, M., Roop, D., Bhowmik, S., Majeski, P., and Conti, C.J. (1994). Expression of keratins in mouse vaginal epithelium. Differentiation *56*, 143–151.

Goad, J., Ko, Y.A., Kumar, M., Syed, S.M., and Tanwar, P.S. (2017). Differential Wnt signaling activity limits epithelial gland development to the anti-mesometrial side of the mouse uterus. Dev. Biol. *423*, 138–151.

Grabherr, M.G., Haas, B.J., Yassour, M., Levin, J.Z., Thompson, D.A., Amit, I., Adiconis, X., Fan, L., Raychowdhury, R., Zeng, Q., et al. (2011). Full-length transcriptome assembly from RNA-Seq data without a reference genome. Nat. Biotechnol. *29*, 644–652.

Hewitt, S.C., and Korach, K.S. (2018). Estrogen Receptors: New Directions in the New Millennium. Endocr. Rev. *39*, 664–675.

Hong, K.U., Reynolds, S.D., Watkins, S., Fuchs, E., and Stripp, B.R. (2004). Basal cells are a multipotent progenitor capable of renewing the bronchial epithelium. Am. J. Pathol. *164*, 577–588.

Huelsken, J., Vogel, R., Erdmann, B., Cotsarelis, G., and Birchmeier, W. (2001). beta-Catenin controls hair follicle morphogenesis and stem cell differentiation in the skin. Cell *105*, 533–545.

Kaushik, G., Ponnusamy, M.P., and Batra, S.K. (2018). Concise Review: Current Status of Three-Dimensional Organoids as Preclinical Models. Stem Cells *36*, 1329–1340.

Kobayashi, A., and Behringer, R.R. (2003). Developmental genetics of the female reproductive tract in mammals. Nat. Rev. Genet. *4*, 969–980.

Kumar, M., and Tanwar, P.S. (2017). Canonical Wnt/β-Catenin Signaling Regulates Postnatal Mouse Epididymal Development But Does Not Affect Epithelial Cell Differentiation. Endocrinology *158*, 4286–4299.

Kurita, T., Cunha, G.R., Robboy, S.J., Mills, A.A., and Medina, R.T. (2005). Differential expression of p63 isoforms in female reproductive organs. Mech. Dev. *122*, 1043–1055.

Lavrik, I., Golks, A., and Krammer, P.H. (2005). Death receptor signaling. J. Cell Sci. *118*, 265–267.

Lee, Y., Dizzell, S.E., Leung, V., Nazli, A., Zahoor, M.A., Fichorova, R.N., and Kaushic, C. (2016). Effects of Female Sex Hormones on Susceptibility to HSV-2 in Vaginal Cells Grown in Air-Liquid Interface. Viruses *8*, E241.

Li, S., Herrera, G.G., Tam, K.K., Lizarraga, J.S., Beedle, M.T., and Winuthayanon, W. (2018). Estrogen Action in the Epithelial Cells of the Mouse Vagina Regulates Neutrophil Infiltration and Vaginal Tissue Integrity. Sci. Rep. *8*, 11247.

Macosko, E.Z., Basu, A., Satija, R., Nemesh, J., Shekhar, K., Goldman, M., Tirosh, I., Bialas, A.R., Kamitaki, N., Martersteck, E.M., et al. (2015). Highly Parallel Genome-wide Expression Profiling of Individual Cells Using Nanoliter Droplets. Cell *161*, 1202–1214.

Mehta, F.F., Son, J., Hewitt, S.C., Jang, E., Lydon, J.P., Korach, K.S., and Chung, S.H. (2016). Distinct functions and regulation of epithelial progesterone receptor in the mouse cervix, vagina, and uterus. Oncotarget *7*, 17455–17467.

Mejetta, S., Morey, L., Pascual, G., Kuebler, B., Mysliwiec, M.R., Lee, Y., Shiekhattar, R., Di Croce, L., and Benitah, S.A. (2011). Jarid2 regulates mouse epidermal stem cell activation and differentiation. EMBO J. *30*, 3635–3646.

Miyagawa, S., and Iguchi, T. (2015). Epithelial estrogen receptor 1 intrinsically mediates squamous differentiation in the mouse vagina. Proc. Natl. Acad. Sci. USA *112*, 12986–12991.

Miyoshi, H., and Stappenbeck, T.S. (2013). In vitro expansion and genetic modification of gastrointestinal stem cells in spheroid culture. Nat. Protoc. *8*, 2471–2482.

Nakamura, T., Miyagawa, S., Katsu, Y., Watanabe, H., Mizutani, T., Sato, T., Morohashi, K., Takeuchi, T., Iguchi, T., and Ohta, Y. (2012). Wnt family genes and their modulation in the ovary-independent and persistent vaginal epithelial cell proliferation and keratinization induced by neonatal diethylstilbestrol exposure in mice. Toxicology *296*, 13–19.

Nusse, R. (2008). Wnt signaling and stem cell control. Cell Res. *18*, 523–527.

Ousset, M., Van Keymeulen, A., Bouvencourt, G., Sharma, N., Achouri, Y., Simons, B.D., and Blanpain, C. (2012). Multipotent and unipotent progenitors contribute to prostate postnatal development. Nat. Cell Biol. *14*, 1131–1138.

Pacal, M., and Bremner, R. (2012). Mapping differentiation kinetics in the mouse retina reveals an extensive period of cell cycle protein expression in post-mitotic newborn neurons. Dev. Dyn. *241*, 1525–1544.

Papafotiou, G., Paraskevopoulou, V., Vasilaki, E., Kanaki, Z., Paschalidis, N., and Klinakis, A. (2016). KRT14 marks a subpopulation of bladder basal cells with pivotal role in regeneration and tumorigenesis. Nat. Commun. *7*, 11914.

Perez-Llamas, C., and Lopez-Bigas, N. (2011). Gitools: analysis and visualisation of genomic data using interactive heat-maps. PLoS ONE *6*, e19541.

Plasschaert, L.W., Žilionis, R., Choo-Wing, R., Savova, V., Knehr, J., Roma, G., Klein, A.M., and Jaffe, A.B. (2018). A single-cell atlas of the airway epithelium reveals the CFTR-rich pulmonary ionocyte. Nature *560*, 377–381.

Rock, J.R., Onaitis, M.W., Rawlins, E.L., Lu, Y., Clark, C.P., Xue, Y., Randell, S.H., and Hogan, B.L. (2009). Basal cells as stem cells of the mouse trachea and human airway epithelium. Proc. Natl. Acad. Sci. USA *106*, 12771–12775.

Salomon, R., Kaczorowski, D., Valdes-Mora, F., Nordon, R.E., Neild, A., Farbehi, N., Bartonicek, N., and Gallego-Ortega, D. (2019). Droplet-based single cell RNAseq tools: a practical guide. Lab Chip *19*, 1706–1727.

Savidis, G., Perreira, J.M., Portmann, J.M., Meraner, P., Guo, Z., Green, S., and Brass, A.L. (2016). The IFITMs Inhibit Zika Virus Replication. Cell Rep. *15*, 2323–2330.

Schneider, C.A., Rasband, W.S., and Eliceiri, K.W. (2012). NIH Image to ImageJ: 25 years of image analysis. Nat. Methods *9*, 671–675.

Sobecki, M., Mrouj, K., Colinge, J., Gerbe, F., Jay, P., Krasinska, L., Dulic, V., and Fisher, D. (2017). Cell-Cycle Regulation Accounts for Variability in Ki-67 Expression Levels. Cancer Res. *77*, 2722–2734.

Soriano, P. (1999). Generalized lacZ expression with the ROSA26 Cre reporter strain. Nat. Genet. *21*, 70–71.

Tanimura, S., Tadokoro, Y., Inomata, K., Binh, N.T., Nishie, W., Yamazaki, S., Nakauchi, H., Tanaka, Y., McMillan, J.R., Sawamura, D., et al. (2011). Hair follicle stem cells provide a functional niche for melanocyte stem cells. Cell Stem Cell *8*, 177–187.

Tanwar, P.S., Zhang, L., Tanaka, Y., Taketo, M.M., Donahoe, P.K., and Teixeira, J.M. (2010). Focal Mullerian duct retention in male mice with constitutively activated beta-catenin expression in the Mullerian duct mesenchyme. Proc. Natl. Acad. Sci. USA *107*, 16142–16147.

Teta, M., Rankin, M.M., Long, S.Y., Stein, G.M., and Kushner, J.A. (2007). Growth and regeneration of adult beta cells does not involve specialized progenitors. Dev. Cell *12*, 817–826.

Tsai, P.S., and Bern, H.A. (1991). Estrogen-independent growth of mouse vaginal epithelium in organ culture. J. Exp. Zool. *259*, 238–245.

Tuttle, A.H., Rankin, M.M., Teta, M., Sartori, D.J., Stein, G.M., Kim, G.J., Virgilio, C., Granger, A., Zhou, D., Long, S.H., et al. (2010). Immunofluorescent detection of two thymidine analogues (CldU and IdU) in primary tissue. J. Vis. Exp. *46*, 2166.

Valdes-Mora, F., Salomon, R., Gloss, B., Law, A.M., Murphy, K., Roden, D.L., Castillo, L., Colino-Sanguino, Y., Kikhtyak, Z., Farbehi, N., et al. (2019). Single-cell RNAseq uncovers involution mimicry as an aberrant development pathway during breast cancer metastasis. bioRxiv. https://doi.org/10.1101/624890.

Vasioukhin, V., Degenstein, L., Wise, B., and Fuchs, E. (1999). The magical touch: genome targeting in epidermal stem cells induced by tamoxifen application to mouse skin. Proc. Natl. Acad. Sci. USA *96*, 8551–8556.

## STAR★METHODS

### KEY RESOURCES TABLE

| REAGENT or RESOURCE | SOURCE | IDENTIFIER |
|---|---|---|
| Antibodies | | |
| Rat anti-BrdU (BU1/75(ICR1)) | Accurate Chemical & Scientific Corporation | Cat#OBT0030G; RRID: AB_609567 |
| Mouse anti-BrdU (B44) | BD Biosciences | Cat#347580; RRID: AB_400326 |
| Mouse anti-βcatenin | BD Transduction Laboratories | Cat#610154; RRID: AB_397555 |
| Rabbit anti-Ki67 | Abcam | Cat#ab15580; RRID: AB_443209 |
| Rabbit Anti-p75 NGF Receptor | Abcam | Cat# ab8875; RRID:AB_306828 |
| Tp63 (H-137) | Santa Cruz Biotechnology | Cat# sc-8343; RRID:AB_653763 |
| Rabbit Anti- Keratin 1 | Covance Research Products Inc | Cat# PRB-165P-100; RRID:AB_291583 |
| Rabbit anti-Keratin 5 | Abcam | Cat# ab52635; RRID:AB_869890 |
| Rabbit anti-Keratin 17 | Abcam | Cat# ab109725; RRID:AB_10889888 |
| Rabbit anti-Filaggrin | BioLegend | Cat# 905801; RRID:AB_2565053 |
| Rabbit anti-Survivin (Birc5) | Cell Signaling Technology | Cat# 2808; RRID:AB_2063948 |
| Rabbit anti- FABP5 | Cell Signaling Technology | Cat# 39926; RRID:AB_2799165 |
| Rabbit anti-IFITM3 | Proteintech Group | Cat# 11714-1-AP; RRID:AB_2295684 |
| Alexa Fluor 488 goat anti-rat IgG (F(ab')$_2$) | Jackson ImmunoResearch Labs | Cat#112-545-072; RRID: AB_2338359 |
| Alexa Fluor 488 goat anti-mouse IgG (F(ab')$_2$) | Jackson ImmunoResearch Labs | Cat#115-545-072; RRID: AB_2338848 |
| Alexa Fluor 594 goat anti-rabbit IgG (F(ab')$_2$) | Jackson ImmunoResearch Labs | Cat#111-585-047; RRID: AB_2338064 |
| Peroxidase goat anti-rabbit IgG (F(ab')$_2$) | Jackson ImmunoResearch Labs | Cat#111-036-047; RRID: AB_2337945 |
| Alexa Fluor 647 goat anti-rabbit IgG (H + L) | Thermo Fisher Scientific | Cat#A-21245; RRID:AB_2535813 |
| Alexa Fluor 555 goat anti-mouse IgG (H + L) | Thermo Fisher Scientific | Cat# A32727; RRID:AB_2633276 |
| Chemicals, Peptides, and Recombinant Proteins | | |
| Pronase | Sigma-Aldrich | Cat#10165921001 |
| DNase I | Sigma-Aldrich | Cat#10104159001 |
| Fetal Bovine Serum | Bovogen | Cat#SFBS-F |
| L-glutamine | HyClone | Cat#SH30034.01 |
| Penicillin-streptomycin | Thermo Fisher Scientific | Cat#15070-063 |
| Matrigel | Trevigen | Cat#3433-010-01 |
| Mouse EGF recombinant | Sigma-Aldrich | Cat#SRP3196 |
| Y-27632 dihydrochloride | Tocris | Cat#1254 |
| SB431542 TGF beta inhibitor | Seleckchem | Cat#S1067 |
| Ultra serum-G | PALL | Cat#15950-017 |
| TrypLE express | Thermo Fisher Scientific (GIBCO) | Cat#12604-021 |
| Doxycycline hyclate (lot#086M4035V) | Sigma-Aldrich | Cat#D9891 |
| Neutral Red | Sigma-Aldrich | 72210 |
| DMEM/F12 HAM | Sigma-Aldrich | Cat#D8437 |
| HBSS/Modified | HyClone | Cat#SH30031.02 |
| Tamoxifen (Lot#SLBF8049V) | Sigma-Aldrich | Cat#T5648; CAS#10540-29-1 |
| β-Estradiol (Lot#SLBH0091V) | Sigma-Aldrich | Cat#E8875; CAS#50-28-2 |
| DAPI dilactate | Sigma-Aldrich | Cat#D9564 |
| Paraformaldehyde 16% solution EM Grade | Electron Microscopy Sciences | Cat#15710 |
| Xgal (Lot#ES531-B061890) | Bioline | Cat#BIO-37035 |
| 5-Chloro-2'-Deoxyuridine (Lot#QR10915) | MP Biochemicals LLC. | Cat#105478; CAS#50-90-8 |
| 5-Iodo-2'-Deoxyuridine (Lot#BCBP3111V) | Sigma-Aldrich | Cat#17152 |

(*Continued on next page*)

*Continued*

| REAGENT or RESOURCE | SOURCE | IDENTIFIER |
|---|---|---|
| Critical Commercial Assays | | |
| RNeasy Micro Kit | QIAGEN | Cat#74004 |
| Qubit 2.0 Fluorometer assay | Invitrogen | N/A |
| RNAscope 2.5 HD Assay-RED kit | ACD | 322350 |
| RNAscope 2.5 HD Detection Reagents-RED | ACD | 322360 |
| RNAscope H202 & Protease Plus Reagents | ACD | 322330 |
| RNAscope Negative Control Probe - DapB | ACD | 310043 |
| RNAscope Positive Control Probe - Mm-Ppib | ACD | 313911 |
| Probe-Mm-Axin2 | ACD | 400331 |
| Probe -Mm-Dkk1 | ACD | 402521 |
| Probe - Mm-Dkk2 | ACD | 404841 |
| Probe -Mm-Dkk3 | ACD | 400931 |
| Probe -Mm-Dkk-4 | ACD | 404851 |
| Probe - Mm-Sfrp2 | ACD | 400381 |
| Probe -Mm-Sfrp4 | ACD | 404991 |
| Probe - Mm-Frzb | ACD | 404861 |
| Probe - Mm-Sfrp1 | ACD | 404981 |
| Probe - Mm-Sfrp5 | ACD | 405001 |
| Probe - Mm-Wif1 | ACD | 412361 |
| Probe - Mm-Wnt1 | ACD | 401091 |
| Probe - Mm-Wnt10a | ACD | 401061 |
| Probe - Mm-Wnt10b | ACD | 401071 |
| Probe - Mm-Wnt2 | ACD | 313601 |
| Probe - Mm-Wnt2b | ACD | 405031 |
| Probe -Mm-Wnt11 | ACD | 405021 |
| Probe -Mm-Wnt16 | ACD | 401081 |
| Probe -Mm-Wnt4 | ACD | 401101 |
| Probe -Mm-Wnt7a | ACD | 401121 |
| Probe -Mm-Wnt7b | ACD | 401131 |
| Probe - Mm-Wnt3 | ACD | 312241 |
| Probe - Mm-Wnt3a | ACD | 405041 |
| Probe - Mm-Wnt5a | ACD | 316791 |
| Probe - Mm-Wnt5b | ACD | 405051 |
| Probe - Mm-Wnt6 | ACD | 40111 |
| Probe - Mm-Wnt8a | ACD | 405061 |
| Probe - Mm-Wnt8b | ACD | 405071 |
| Probe - Mm-Wnt9a | ACD | 405081 |
| Probe - Mm-Wnt9b | ACD | 405091 |
| Deposited Data | | |
| scRNA-seq data | This paper | GEO: GSE142212 |
| Experimental Models: Cell Lines | | |
| L-WRN cells | ATCC | Cat#CRL-3276; RRID: CVCL_DA06 |
| Experimental Models: Organisms/Strains | | |
| Mouse STOCK Tg(KRT14-cre/ERT)20Efu/J | The Jackson laboratory | JAX:005107, RRID:IMSR_JAX:005107 |
| Mouse: *Axin2*$^{rtTA}$: B6.Cg-Tg(Axin2-rtTA2S*M2)7Cos/J | The Jackson Laboratory | JAX:016997; RRID:IMSR_JAX:016997 |
| Mouse: *tetO*$^{Cre}$: STOCK Tg(tetO-cre)1Jaw/J | The Jackson Laboratory | JAX:006224; RRID:IMSR_JAX:006224 |
| Mouse: *tetO*$^{H2BJGFP}$: STOCK Tg(tetO-HIST1H2BJ/GFP)47Efu/J | The Jackson Laboratory | JAX:005104; RRID:IMSR_JAX:005104 |

(*Continued on next page*)

| Continued | | |
|---|---|---|
| REAGENT or RESOURCE | SOURCE | IDENTIFIER |
| Mouse: *R26-lacZ*$^{fl/fl}$: B6.129S4-Gt(ROSA)26Sor$^{tm1Sor}$/J | The Jackson Laboratory | JAX:003474; RRID:IMSR_JAX:003474 |
| Mouse: *Ctnnb1*$^{fl/fl}$: B6.129-Ctnnb1$^{tm2Kem}$/KnwJ | The Jackson Laboratory | JAX:004152; RRID:IMSR_JAX:004152 |
| Oligonucleotides | | |
| Mouse *Gapdh* Forward# TGGCAAAGTGGAGATTGTTGCC | Bonnans et al., 2012 | N/A |
| Mouse *Gapdh* Reverse# AAGATGGTGATGGGCTTCCCG | Bonnans et al., 2012 | N/A |
| Mouse *Axin2* Forward# CGACCCAGTCAATCCTTATCAC | Boretto et al., 2017 | N/A |
| Mouse *Axin2* Reverse# GGGACTCCATCTACGCTACTG | Boretto et al., 2017 | N/A |
| Mouse *Keratin1* Forward# GACACCACAACCCGGAC CCAAAACTTAG | Mejetta et al., 2011 | N/A |
| Mouse *Keratin1* Reverse# ATACTGGGCCTTGACTTCC GAGATGATG | Mejetta et al., 2011 | N/A |
| Mouse *Filaggrin* Forward# GGAGGCATGGTGGAACTGA | Mejetta et al., 2011 | N/A |
| Mouse *Filaggrin* Reverse# TGTTTATCTTTTCCCTCAC TTCTACATC | Mejetta et al., 2011 | N/A |
| Mouse *Ctnnb1 Forward#* AGACAGCTCGTTGTACTGCT | Kumar and Tanwar, 2017 | N/A |
| Mouse *Ctnnb1 Reverse#* GTGTCGTGATGGCGTAGAAC | Kumar and Tanwar, 2017 | N/A |
| Software and Algorithms | | |
| Proteome Discoverer software version 2.1 | Thermo Fisher Scientific | N/A |
| Gitools 2.3.1 software | Perez-Llamas and Lopez-Bigas, 2011 | http://www.gitools.org |
| ImageJ | Schneider et al., 2012 | https://imagej.nih.gov/ij/ |
| GraphPad Prism version 7.02 | GraphPad Software, La Jolla California USA | https://www.graphpad.com |

## LEAD CONTACT AND MATERIALS AVAILABILITY

Further information and requests for resources and reagents should be directed to and will be fulfilled by the Lead Contact, Assoc. Prof. Pradeep Tanwar (Pradeep.tanwar@newcastle.edu.au). All unique/stable reagents generated in this study are available from the Lead Contact without restriction.

## EXPERIMENTAL MODEL AND SUBJECT DETAILS

### Mice

All the experimental procedures with mice were approved by the Animal Care and Ethics Committee of The University of Newcastle, Australia. The guidelines of New South Wales Animal Research Act, New South Wales Animal Research Regulation, and the Australian Code for the care and use of animals for the scientific purposes, were followed for animals' care and experimental procedures. All the animals were maintained on C57BL/6; 129SvEv mixed genetic background. Mice had access to food and water *ad libitum* and were maintained under 12-hour dark/light cycle. For tracing the fate of vaginal epithelium, *K14Cre*$^{ERT2}$ (Vasioukhin et al., 1999) mice were bred with *Gt(ROSA)26Sor*$^{tm1Sor/J}$ *(lacZ*$^{fl/fl}$*)* (Soriano, 1999) to generate *K14Cre*$^{ERT2}$/*lacZ*$^{fl/+}$ mice. For deletion of βcatenin gene (*Ctnnb1*) in vaginal epithelium, *K14Cre*$^{ERT2}$ mice were bred with *Ctnnb1*$^{fl/fl}$ (Huelsken et al., 2001) mice to generate *K14Cre*$^{ERT2}$/*Ctnnb1*$^{fl/fl}$ mice. For tracing lineage of Axin2-expressing cells, *Axin2*$^{rtTA}$/*tetO*$^{Cre}$ mice were bred with *lacZ*$^{fl/fl}$ mice to generate *Axin2*$^{rtTA}$/*tetO*$^{Cre}$/*lacZ*$^{fl/+}$ mice. For genotyping, DNA was extracted from mice ear clips using REDExtract-N-Amp Tissue PCR Kit (Sigma) and PCRs were performed using a standard protocol (Goad et al., 2017). *Axin2*$^{rtTA}$ mice were bred with *tetO*$^{H2BJGFP}$ mice to generate *Axin2*$^{rtTA}$/*tetO*$^{H2BJGFP}$ mice. For single cell RNaseq analysis, vaginal epithelial cells were isolated from 6w old adult C57Bl6 wild-type mice and ovariectomized (OVX) mice.

### Epithelial cell isolation and organoid culture

The vaginae of 6w old adult mice were dissected out, washed with $Ca^{2+}$ and $Mg^{2+}$ free Hanks Balanced Salt Solution (HBSS), and were slit open to expose the epithelium during subsequent enzymatic digestion. The tissues were placed in DMEM/F12 containing 1mg/ml Pronase (Sigma) and 0.5mg/ml DNase1 (Sigma) at 4°C overnight with slow shaking. Enzymatic digestion was stopped by adding DMEM/F12 medium (Sigma) supplemented with 10% fetal bovine serum (Bovogen). The epithelium was then squeezed out with the help of a pair of forceps under the dissecting microscope. Following two successive washes in DMEM/F12, the single

cell suspension was prepared using 40μm cell strainer before plating. For organoid culture, 10,000 cells were resuspended in 25μl Matrigel and cultured in DMEM/F12 supplemented with 2% Ultraserum-G (PALL Corporation), 1% Penicillin-Streptomycin (Lonza), 50ng/ml mouse EGF (Sigma), 0.5μM A83-01 (TGFβ/Alk inhibitor) (Sellekchem) and 10μM Y-27632 dihydrochloride (ROCK inhibitor) (Tocris). The medium was changed every 2 days. The organoids were imaged on JuLiTM Stage Real-Time Cell History Recorder (NanoEnTek, ROK) at different time points, and the number of organoids formed was quantified using ImageJ (NIH).

*Axin2*$^{rtTA}$/ *tetO*$^{H2BJGFP}$ mice were used for FACS sorting of GFP$^{+}$ (Axin2$^{+}$) and GFP$^{-}$ (Axin2$^{-}$) cells. FACS sorting was performed on a FACSAria2 sorter using the FACS DiVa (software version 6.1.3) (BD Biosciences). Dead cells were excluded with propidium iodide. FACS sorted cells were resuspended in Matrigel and cultured in DMEM/F12 complete media.

To study the effect of E2 on organoids, cells were isolated from vaginae of 6w old adult mice and were culture in media supplemented with 100ng/ml β-estradiol (Sigma).

For long term organoid culture of cells, media was changed every 3 days and passaging was done every 10 days. Briefly, Matrigel droplets containing organoids were dissolved in ice-cold DPBS. Organoids were dissociated into single cells by incubation in TrypLE express (Thermo Fisher Scientific) at 37C for 10 mins. Trypsinization was stopped by adding DMEM/F12 medium supplemented with 10% fetal bovine serum. Cell clumps were further dissociated into single cells by gentle pipetting and were reseeded in Matrigel droplets.

For modulation of Wnt signaling, organoids were cultured in complete media supplemented with WRN conditioned media at various concentrations of 5%, 10%, 25% and 50%.

### Cell lines

The L-WRN cell line (ATCC CRL-3276) expressing Wnt3A, Rspondin3 and noggin was used for producing WRN conditioned medium (Miyoshi and Stappenbeck, 2013).

## METHOD DETAILS

### Targeting lacZ expression

*K14Cre*$^{ERT2}$/*lacZ*$^{fl/+}$ and *Axin2*$^{rtTA}$/*tetO*$^{Cre}$/*lacZ*$^{fl/+}$ female mice express lacZ-encoded β galactosidase in all cells derived from K14-expressing cells and Axin2-expressing cells, respectively.

For lineage tracing, 6w-old *K14Cre*$^{ERT2}$/*lacZ*$^{fl/+}$ mice were injected with tamoxifen (2mg per mouse per day) intraperitoneally for three alternate days. Upon tamoxifen administration, *K14Cre*$^{ERT2}$/*lacZ*$^{fl/+}$ express *lacZ* (βgal) in K14-expressing cells and their progenies. *K14Cre*$^{ERT2}$/*Ctnnb1*$^{fl/+}$ were injected with tamoxifen (1mg per mouse per day) intraperitoneally for 5 consecutive days to induce deletion of *Ctnnb1* (*Ctnnb1*$^{cko}$) from K14 expressing cells and their progenies. For regeneration experiment, *K14Cre*$^{ERT2}$/*lacZ*$^{fl/+}$ mice were ovariectomized at 6w age, and allowed to recover for 2w, after which they were induced with a single dose of 5mg tamoxifen intraperitoneally. Mice vaginae were collected at different time points for further analysis.

For lineage tracing, 6w old *Axin2*$^{rtTA}$/*tetO*$^{Cre}$/*lacZ*$^{fl/+}$ mice were induced by feeding doxycycline in drinking water (5 mg/ml, supplemented with 5% sucrose) for 3w. To initiate labeling at single cell density, and subsequent lineage tracing, *Axin2*$^{rtTA}$/*tetO*$^{Cre}$/*lacZ*$^{fl/+}$ female mice were induced with 2mg of doxycycline (dissolved in sterile PBS) by intraperitoneal injection at 6w of age. For regeneration experiment, *Axin2*$^{rtTA}$/*tetO*$^{Cre}$/*lacZ*$^{fl/+}$ were ovariectomized (OVX) at 6w of age, and allowed to recover for 2w, after which doxycycline was administered to induce labeling at single cell density. Ten days after doxycycline administration, *Axin2*$^{rtTA}$/*tetO*$^{Cre}$/*lacZ*$^{fl/+}$ mice were further injected subcutaneously with 400 ng 17β-oestradiol (Sigma) dissolved in sesame oil (four injections of 100ng every day) to allow regeneration of hormone-deprivation induced atrophied vagina. Mice were sacrificed 24 hours after the last injection and processed for tissue collection. Littermates were used as the control for all experiments.

### Histology and immunostaining

Vaginal tissues collected from different mice were fixed in 4% paraformaldehyde at 4°C overnight and then processed for paraffin embedding. IF/IHC were performed as described in Ghosh et al. (2017). The following primary antibodies were used rabbit anti-Tp63 (1:500), rabbit anti-Ki67 (1:500), rabbit anti-keratin 1 (1:500), rabbit anti-filaggrin (1:500), mouse anti-β-catenin (1:200), rabbit Anti-p75 NGF Receptor (1:250), rabbit anti-keratin5 (1:1000), rabbit anti-keratin17 (1:250), rabbit anti-survivin (Birc5) (1:250), rabbit anti-FABP5 (1:500), rabbit anti-IFITM3 (1:500). The following secondary antibodies were used: anti-rabbit, anti-rat, anti-mouse conjugated to HRP or AlexaFluor 488/594 (1:250), anti-rabbit conjugated to AlexaFluor 647 (1:250) and anti-mouse conjugated to Alexafluor 555 (1:250). For immunofluorescence, nuclei were stained with 4', 6-diamidino-2-phenylindole (DAPI) and mounted in buffered glycerol. For immunohistochemistry, EnVisionTM+ Dual Link System-HRP (DAB+) kit was used as per manufacturer instructions. Nuclei were counterstained with hematoxylin and mounted in toluene-based Cytoseal mounting medium (ProSciTech).

### Beta-galactosidase/X-gal staining

X-gal staining for the presence of β-galactosidase/LacZ activity has been described previously (Ghosh et al., 2017). Briefly, vaginae from *K14Cre*$^{ERT2}$/*lacZ*$^{fl/+}$ and *Axin2*$^{rtTA}$/*tetO*$^{Cre}$/*lacZ*$^{fl/+}$ female mice were fixed in 4% paraformaldehyde (PFA) at 4°C for 1h. Vaginal tissue slices of 125μm thickness were prepared using McIlwain Tissue Chopper. Post-fixed tissues were washed 3 times in rinse buffer [0.1% sodium deoxycholate, 0.2% NP40, 2mM MgCl2 in 0.1M phosphate buffer (pH 7.3)] for 30 minutes each at room

temperature. The sections were incubated in X-gal solution for 20-24h at room temperature, followed by fixation in 4% PFA at 4°C overnight, and processed for paraffin embedding. Tissue sections were cut at 8μm thickness and counterstained with nuclear fast red. Combined X-gal/immunostaining procedures were performed on 6 μm tissue sections as per standard immunostaining protocol.

### CldU-IdU labeling

CldU and IdU were dissolved in sterile PBS and injected intra-peritoneally into mice at a dose of 100mg/kg. To test the specificity of these two antisera, we labeled 6w old female mice sequentially with CldU and then IdU (Figure S2). For labeling, mice received intra-peritoneal injection of CldU and IdU (100μg/g body weight, made up as 10mg/ml in PBS) and tissues were analyzed 24h later. Due to the well-established location of the rapidly dividing progenitors (stem/transit amplifying compartments), we used intestines for these labeling strategies. Cells that had undergone replication during the first labeling period when CldU was given (Figure S2) were positive for CldU. Such cells were located in the middle of the villi. Presumably this first cell division occurred within crypts and subsequently the cells migrated up the villi. On the other hand, DNA analog injected later, IdU, was more localized in the crypt bases in which recently dividing cells are presumably located (Figure S2b). Importantly, CldU-IdU co-positive epithelial cells were present within the crypts (Figure S2), where stem/TA compartment is known to exist. These results confirmed the specificity of anti-CldU and anti-IdU antisera.

For IdU label dilution, 6w old female mice were given access to water supplemented with 1mg/ml IdU *ad libitum* for up to 7d (Figure 3B). For short-term labeling, 6w old female mice received intraperitoneal injections of CldU (100μg/g body weight, made up as 10mg/ml in PBS) and IdU (100μg/g body weight, made up as 10mg/ml in PBS) on consecutive days and were sacrificed 24h later (Figure 3C). For long-term labeling in OVX mice, 6w old female mice were first ovariectomized. After recovery period of 14d, mice were given access to water supplemented with 1mg/ml CldU *ad libitum* for up to 2w. This was followed by a washout period of 5d, after which mice were given access to water supplemented with 1mg/ml IdU *ad libitum* for another 2w, and then sacrificed 24h later (Figure 3D). Bottles containing CldU and IdU water were changed every 3d and were covered with aluminum foil to prevent light exposure.

Immunostaining for CldU and IdU was performed as described previously (Tuttle et al., 2010). Briefly, 5 μm paraffin embedded tissue sections were deparaffinized, rehydrated, heated to 110°C for 30 min in 1 mM EDTA buffer (pH 8.0) for antigen retrieval, permeabilized with 0.2% Triton, incubated in 1.5 N HCl, incubated in blocking buffer (10% Normal Goat Serum/ 0.1% Triton in PBS) for 1 h at room temperature, before an overnight incubation for IdU with mouse anti-BrdU antisera (mouse, 1:250). Sections were then washed and incubated overnight with rabbit anti-Tp63 antisera (1:500) and rat anti-BrdU antisera (1:250) for CldU, followed by incubation with secondary antibodies conjugated to AlexaFluor 488, AlexaFluor 594 and AlexaFluor 647. Nuclei were stained with 4', 6-diamidino-2-phenylindole (DAPI) and mounted in buffered glycerol.

### Vaginal epithelial protein isolation and digestion for proteomic analysis

Vaginal epithelial protein preparations from three respective conditions of *Ctnnb1* (βcatenin) deletion after 1w, 2w, and 8w (n = 3 per time point) of tamoxifen treatment were generated for analysis. Vaginal epithelial tissues were then resuspended in ice-cold lysis buffer containing 0.1 M $Na_2CO_3$ pH 11.3 supplemented with protease (Sigma) and phosphatase inhibitors (Roche, IN, USA). Tissue samples were homogenized using a beadbug homogenizer (Benchmark Scientific) until a homogeneous suspension is obtained, and incubated for 1h at 4°C. The soluble proteins were then dissolved in 6M urea and 2M thiourea, reduced with 10 mM dithiothreitol (DTT) for 30 minutes at room temperature and subsequently, alkylated using 20 mM iodoacetamide (Sigma) in the dark for 30 minutes. Proteins were then digested with Lys-C/trypsin (Promega) at a protease-to-protein ratio of 1:25 at room temperature for 3h. Afterward, samples were diluted with 50 mM triethylammonium bicarbonate, pH 7.8 to reduce the urea concentration to 0.75 M and were digested overnight at room temperature. Desalting of peptide was carried out using the solid phase extraction (SPE) columns (Oasis PRIME HLB, Waters, Rydalmere) and a vacuum manifold (Supelco) according to manufacturer's instructions. Peptide concentrations were determined using a Qubit 2.0 Fluorometer assay (Invitrogen).

### Mass spectrometry and database searching

For LC-MS/MS processing, digested peptide solutions were first dried down in a SpeedVac SC100 (Thermo Fisher Scientific), resolubilized in 2% acetonitrile/0.1% trifluoroacetic acid. 500 ng of each peptide sample were measured using nanoflow LC instrument interfaced to a Q Exactive Plus Orbitrap mass spectrometer (Thermo Fisher Scientific), which is equipped with a nanoelectrospray ion source. Peptides were loaded onto a trapping column (Acclaim PepMapTM100, 100 μm x 2 cm, nanoViper fitting C18, 5 μm, 100 Å, Thermo Fisher Scientific) for pre-concentration, and then resolved in the analytical column (EASY-Spray Column, PepMap, 75 μm x 25 cm, nanoviper fitting, C18, 2 μm, 100 Å, Thermo Fisher Scientific) for peptide separation. Solvent A was 0.1% formic acid in HPLC water, and solvent B was 0.1% formic acid in acetonitrile (Acn). The separation of the peptides was achieved at a constant flow rate of 250 nl/min using a linear gradient from 2% to 35% of solvent B over 95 minutes. Ions were generated by positive electrospray ionization via liquid junction into a Q Exactive mass spectrometer. Mass spectra were acquired over m/z 380 – 2,000 at 70,000 resolution and data-dependent acquisition selected the top twenty most abundant precursor ions for tandem mass spectrometry by HCD fragmentation, collision energy of 32.0, and a resolution of 35,000. Dynamic exclusion was set at 15 s, as well as rejection of precursor ions with charge state +1, were employed to minimize redundant MS/MS collection and maximize peptide identifications. The MS raw files were processed using Proteome Discoverer (PD) software (version 2.1, Thermo Fisher Scientific) were search against the

mouse protein database (updated to April 2018). The mass tolerance of precursor mass and fragment mass were set as 10 ppm and 0.02 Da respectively. S-carbamidomethylation of cysteine was set as a fixed modification and asparagine deamidated as dynamic modifications. For digestion, trypsin was set as the digestion enzyme with two missed cleavage permitted. A fixed false discovery rate (FDR) was set at < 1% for identification of peptides and proteins. Only keratin and filaggrin proteins represented by at least two unique peptides were included in the analysis. Data were analyzed using Gitools 2.3.1 software to generate heatmaps and a protein is considered upregulated if the level of expression was 1.5-fold higher than the 1w β-catenin deletion and downregulated if it was 0.66-fold lower than the 1w β-catenin deletion.

### *In Situ* Hybridization (ISH)

ISH was performed as described in Goad et al. (2017). Vaginae were collected from 4w-old mice (n = 4) and 6w old adult mice across the estrus cycle stages (n = 3). Tissues were fixed in 10% buffered formalin (Sigma) for 24h at room temperature and then processed for paraffin embedding and sectioned at 4μm thickness. Probe details in the key resource table.

### Wnt Signaling qPCR arrays

Total RNA was extracted from 6w old adult OVX and E2-treated vaginal tissues using QIAGEN RNeasy® Micro kit as per manufacturer's instructions (QIAGEN). RNA was quantified and equal concentrations used for cDNA synthesis with RT2 First Strand Kit (QIAGEN). QPCR was then performed using RT2 SYBR Green ROX qPCR Mastermix (QIAGEN) and RT2 Profiler PCR Array Kit (QIAGEN) on ABI 7900 HT FAST (Applied Biosciences) as described in Goad et al. (2017). Data were analyzed as per manufacturer's instructions, and the reactions were normalized against the five housekeeping genes included in the arrays. To study the mRNA expression levels for *Ctnnb1*, *K1* and *Flg*, RNA was isolated from the vaginal epithelium of $Ctnnb1^{fl/fl}$ and $Ctnnb1^{cko}$ using the RNeasy Micro Kit (QIAGEN) following the manufacturer's instructions. qRT-PCR was performed as detailed in Ghosh et al. (2017).

### Microscope image acquisition

Images of immunostaining were acquired with Olympus BX51 upright fluorescence microscope equipped with Olympus UPlanFLN objectives (x40, NA = 0.75; x60, NA = 0.9) and Olympus DP72 CCD (charge-coupled device) color camera using cellSens software (Olympus), or Zeiss AxioImager A1 upright fluorescence microscope equipped with AxioCam MRc camera and Zeiss EC Plan-NEOFLUAR objectives (x20, NA = 0.5; x40, NA = 0.75) using ZEN software or Olympus Fluoview FV10i upright confocal laser scanning microscope fitted with 60x oil-immersion objective (NA = 1.35) (Olympus), using FV10i-SW software. Whole mount imaging of 100um thick slices of X-gal stained vaginae was done on SMZ25 stereoscope equipped with Nikon DS-Fi2 camera and Nikon P2-SHR Plan Apo 2X objective (NA = 0.312). Images consisted of 15–30 stacks with variable *z*-spacing and were captured and merged using NIS-Elements software. All images were captured at room temperature.

## QUANTIFICATION AND STATISTICAL ANALYSIS

### Single Cell RNaseq analysis

Single cell RNaseq was performed using the Dropseq as previously described (Macosko et al., 2015). The sequencing output was analyzed using the McCaroll lab cookbook a custom genome (mm10 plus Trinity assemblies of transgene sequences) (Grabherr et al., 2011) and gene annotation (gencode vM14 plus). Seurat (v Seurat_2.3.4 (Butler et al., 2018) was the main platform for downstream analysis. Briefly DGE matrices were trimmed for quality metrics (> 100 genes, < 15% mitochondrial reads, < 1200 UMI and genes expressed in at least 3 cells). Evaluation of potential batch effect was performed by PCA visualization in the first 3 dimensions and outlier experiments were omitted. QC filtering resulted in expression data for 4912 cells in wild-type with a median of 813 genes per cell and 3527 cells in OVX with a median of 405 genes per cell. Downstream analysis was performed according to Butler et al. with UMI number regression and 20 principal components of variable genes being used for dimensional reduction (TSNE) and cluster calling (Butler et al., 2018). We subsequently removed outlier cells that contained more than 4,000 genes as they could potentially constitute cell doublets. Analysis were performed as described previously in Valdes-Mora et al. (2019).

For comparative analysis between OVX and wild-type scRNA-seq data: Downstream analysis was performed according to Butler et al. with UMI number regression (Butler et al., 2018). Canonical correction analysis (CCA) was performed between replicates to remove batch effect using the union of the top 1000 variable genes of each replicate. We removed cells where the variance explained by CCA is less than 2-fold compared to PCA. 10 CC dimensions for wild-type and 6 for OVX were used to aligned data and dimensional reduction (tSNE). For combined analysis wild-type cells and OVX cells were merged and 15 principal components of variable genes were used for tSNE representation.

### Statistical Analysis

All statistical analyses were performed on GraphPad Prism (v.7.02). Data are presented as mean ± s.e.m. Statistical analyses was done using two-tailed Student's t test, one-way ANOVA or two-way ANOVA with multiple comparisons to determine significance in two-group and multiple-group experiments, respectively. Further details of statistical analysis and the number of mice analyzed is included in figure legends.

## DATA AND CODE AVAILABILITY

Quantitative data supporting the figures is described in the paper. The scRNA-seq data of the vaginal epithelial cells discussed in this publication have been deposited in NCBI's Gene Expression Omnibus (Edgar, 2002) and are accessible through GEO Series accession number GSE142212 (https://www.ncbi.nlm.nih.gov/geo/query/acc.cgi?acc=GSE142212). Additional data files will be made available upon reasonable request from the corresponding author.